Clinical Science (2014) **127**, 435–448 (Printed in Great Britain) doi: 10.1042/CS20130716

online data

Original Paper

SUPPLEMENTARY ONLINE DATA

Disruption of histamine H_2 receptor slows heart failure progression through reducing myocardial apoptosis and fibrosis

Zhi ZENG*, Liang SHEN*, Xixian LI*, Tao LUO*, Xuan WEI*, Jingwen ZHANG*, Shiping CAO*, Xiaobo HUANG*, Yasushi FUKUSHIMA†, Jianping BIN*, Masafumi KITAKAZE*‡, Dingli XU* and Yulin LIAO*

*The State Key Laboratory of Organ Failure Research, Department of Cardiology, Nanfang Hospital, Southern Medical University, Guangzhou, China
†The Department of Internal Medicine, Graduate School of Medicine, University of Tokyo, Bunkyo-ku, Tokyo, Japan
‡Cardiovascular Division of the Department of Medicine, National Cerebral and Cardiovascular Center, Suita, Osaka, Japan

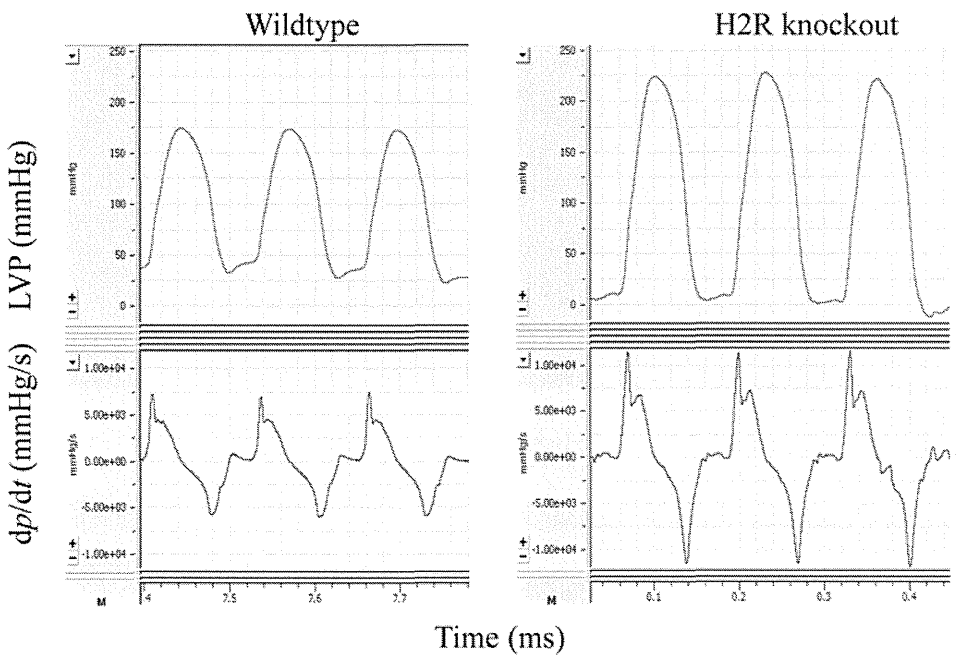

Figure S1 **Examples of LV haemodynamic recording in mice receiving aortic banding for 4 weeks**
d*p*/d*t*, rates of change of LV pressure; LVP, left ventricular pressure.

Correspondence: Dr Yulin Liao (email Liao18@msn.com).

© The Authors Journal compilation © 2014 Biochemical Society

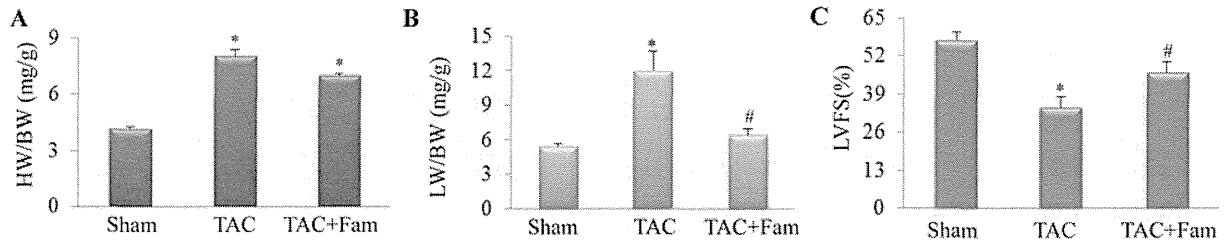

Figure S2 **Famotidine (Fam; 10 mg/kg per day) treatment for 4 weeks improved HF induced by TAC in C57 mice**
(**A**) Heart weight/body weight (HW/BW) ratio. (**B**) Lung weight/BW ratio. (**C**) LVFS.*$P < 0.01$ compared with sham; #$P < 0.05$ compared with TAC; $n = 6$, 9 and 6 in sham, TAC and TAC+Fam groups, respectively.

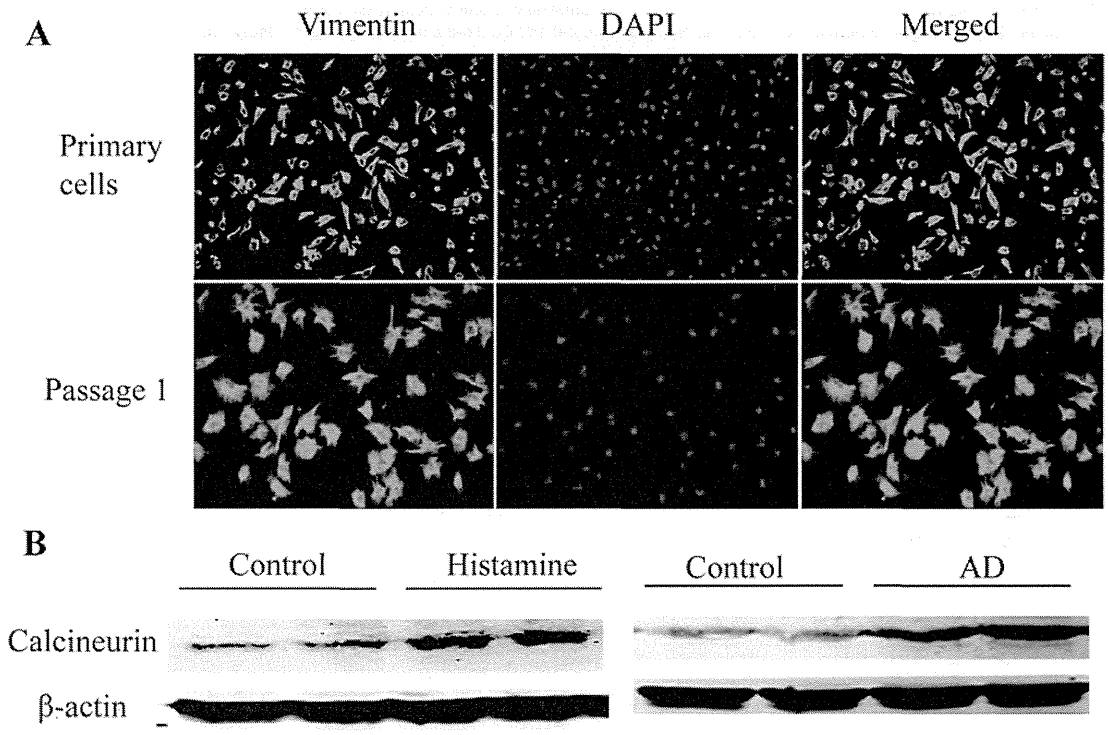

Figure S3 **Fibroblast identification and Western blot analysis of calcineurin in neonatal rat fibroblasts**
(**A**) Vimentin staining was used as a fibroblast marker. (**B**) Western blot analysis of calcineurin. β-Actin was used as loading control. Doses of histamine and AD were 1 μM.

© The Authors Journal compilation © 2014 Biochemical Society

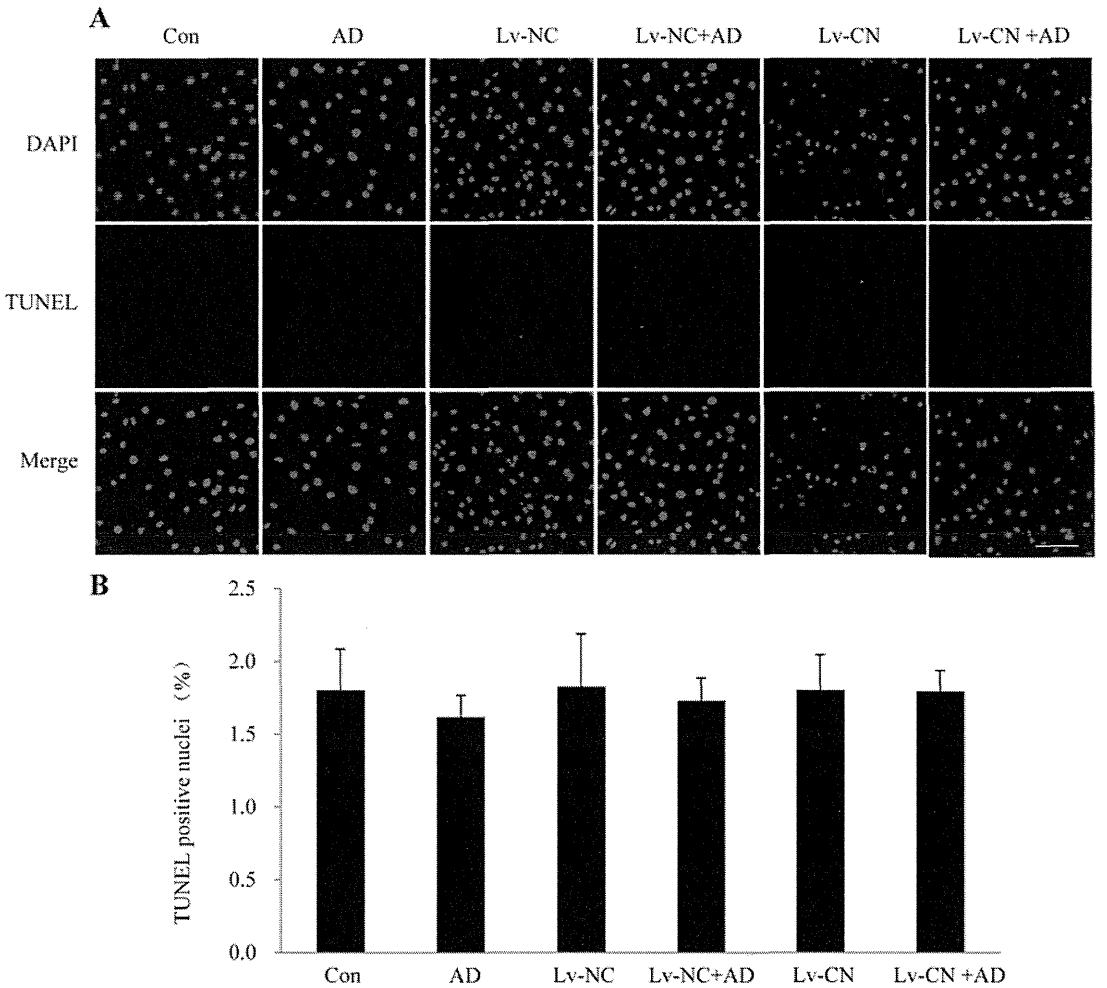

Figure S4 **H2R activation exerted no effect on apoptosis in neonatal rat fibroblasts**
(**A**) TUNEL assay shows that both AD (1 μM) and lentivirus carrying shRNA of calcineurin (Lv-CN) did not influence apoptosis of fibroblasts (pink indicates apoptosis). (**B**) Quantitative analysis of TUNEL. Data are shown as the means $\pm$ S.E.M. Experiments were repeated three times. Scale bar = 75 μm.

Table S1 **Sequences of the primers for routine or real-time PCR or genotyping**
WT, wild-type.

Transcripts	Forward primer (5′→3′)	Reverse primer (5′→3′)	Size (bp)
WT H2R	AATGTGGTCGTCTGCCTGGCT	CTCTGTTGAGGGTGGCGTAC	298
Mutant H2R	ACATCTAGCTTCCTCACTGCCTC	CTGACTAGGGGAGGAGTAGAA	1000
Procollagen I	CTCGTCACAGCCTTCAC	AATCCAGTAGTAATCGCTCTTC	176
Procollagen III	CTACACCTGCTCCTGTCATT	CCACCCATTCCTCCGACT	232
GAPDH	ACCAACTGCTTAGCCCCCC	GCATGTCAGATCCACAACGG	281

Received 5 November 2013/21 February 2014; accepted 21 March 2014
Published as Immediate Publication 21 March 2014, doi: 10.1042/CS20130716

© The Authors Journal compilation © 2014 Biochemical Society

Am J Physiol Heart Circ Physiol 307: H1504–H1511, 2014.
First published September 12, 2014; doi:10.1152/ajpheart.00331.2014.

Pathophysiological impact of serum fibroblast growth factor 23 in patients with nonischemic cardiac disease and early chronic kidney disease

Miki Imazu,[1]* Hiroyuki Takahama,[1]* Hiroshi Asanuma,[2] Akira Funada,[1] Yasuo Sugano,[1] Takahiro Ohara,[1] Takuya Hasegawa,[1] Masanori Asakura,[1,3] Hideaki Kanzaki,[1] Toshihisa Anzai,[1] and Masafumi Kitakaze[1,3]

[1]*Department of Cardiovascular Medicine, National Cerebral and Cardiovascular Center, Suita, Osaka, Japan;* [2]*Department of Cardiovascular Dynamics, National Cerebral and Cardiovascular Center, Suita, Osaka, Japan; and* [3]*Department of Clinical Research and Development, National Cerebral and Cardiovascular Center, Suita, Osaka, Japan*

Submitted 19 May 2014; accepted in final form 3 September 2014

Imazu M, Takahama H, Asanuma H, Funada A, Sugano Y, Ohara T, Hasegawa T, Asakura M, Kanzaki H, Anzai T, Kitakaze M. Pathophysiological impact of serum fibroblast growth factor 23 in patients with nonischemic cardiac disease and early chronic kidney disease. *Am J Physiol Heart Circ Physiol* 307: H1504–H1511, 2014. First published September 12, 2014; doi:10.1152/ajpheart.00331.2014.—Although the important role of fibroblast growth factor (FGF)23 on cardiac remodeling has been suggested in advanced chronic kidney disease (CKD), little is known about serum (s)FGF23 levels in patients with heart failure (HF) due to nonischemic cardiac disease (NICD) and early CKD. The present study aimed to investigate sFGF23 levels in NICD patients and identify the responsible factors for the elevation of sFGF23 levels. We prospectively measured sFGF23 levels in consecutive hospitalized NICD patients with early CKD (estimated glomerular filtration rate $\geq$ 40 ml·min^{-1}·1.73 m^{-2}) and analyzed the data of both echocardiography and right heart catheterization. Of the 156 NICD patients (estimated glomerular filtration rate range: 41–128 ml·min^{-1}·1.73 m^{-2}), the most severe HF symptom (New York Heart Association class III-IV, 53% vs. 33%, $P = 0.015$) was found in the above median sFGF23 (39.1 pg/ml) group compared with the below median sFGF23 group. sFGF23 levels were higher in patients with HF hospitalization history compared with those without HF [median: 46.8 (interquartile range: 38.8–62.7) vs. 34.7 (interquartile range: 29.6–42.4) pg/ml, $P < 0.0001$]. In the multivariate analysis, HF hospitalization was independently related to elevated sFGF23 levels ($P = 0.022$). Both systolic dysfunction and high plasma aldosterone concentration were identified as predictors of high sFGF23 levels ($P < 0.05$). Among the neurohormonal parameters, elevated sFGF23 levels were the only factor to predict a declining left ventricular ejection fraction ($P = 0.001$). These findings suggest that the progression of HF per se contributes to the elevation of sFGF23 levels even in the early stages of CKD, which leads to further myocardial dysfunction, potentially creating a vicious cycle.

fibroblast growth factor 23; heart failure; chronic kidney disease

FIBROBLAST GROWTH FACTOR (FGF)23, a phosphate-regulating hormone secreted from osteoblasts, promotes urinary phosphorus excretion and inhibits the activation of vitamin D in the presence of its cofactor, Klotho (1, 11, 21). Recent studies have suggested that an elevated circulating FGF23 level is an independent risk factor for mortality and morbidity in patients with chronic kidney disease (CKD) (8, 12) and a potential risk factor for cardiovascular events in a community-based population (10). Furthermore, a recent experimental study (4) has demonstrated that FGF23 directly promotes cardiomyocyte hypertrophy. Several clinical studies have also suggested the relationship of serum FGF23 levels with both cardiac dysfunction (25) and hypertrophy in CKD patients (7) and the association between serum FGF23 levels and clinical outcomes in outpatients with stable heart failure (HF) (20). Interestingly, the previous studies have suggested no relationship of FGF23 levels with the prevalence of coronary artery disease (CAD) (25) and coronary artery calcification (24). These clinical and experimental findings have the significant implication that FGF23 can directly influence cardiac function and structure other than the ischemic mechanisms. These findings facilitated us to hypothesize that FGF23 plays a role on the progression of cardiac dysfunction in patients with nonischemic cardiac disease (NICD). In addition, other studies (6, 28) have also reported that circulating FGF23 levels are elevated before the development of overt hyperphosphatemia in the early stages of CKD. These lines of evidence promoted us to test the idea that serum FGF23 levels are elevated even in early stages of CKD and affect the pathophysiology in HF patients. Furthermore, it is also crucial to identify the risk factor to elevated FGF23 levels in HF patients, although the determinants of serum FGF23 levels in NICD patients have not yet been completely identified in the clinical setting.

Accordingly, we measured serum FGF23 levels in NICD patients without advanced renal impairment, surveyed the relationship of serum FGF23 levels with cardiac structure, function, and the hemodynamic state, and sought to identify the determinants of serum FGF23 levels in NICD patients.

METHODS

Study design. This study was a prospective cross-sectional study of serum FGF23 levels in hospitalized patients with NICD at a single center.

NICD patients. Since previous studies have suggested that serum FGF23 levels increased marginally with declining renal function below 30–40 ml/min of glomerular filtration rate (GFR) (13, 28), we set the inclusion criteria for renal function as an estimated GFR (eGFR) of $\geq$40 ml·min^{-1}·1.73 m^{-2}. We could obtain written informed consents from a total of 181 consecutive patients admitted to our department between January and December 2012 (male patients: $n = 93$, 51.4%; female patients: $n = 88$, 48.6%). Patients with CAD were excluded from this study. All patients received coronary angiography or coronary computed tomography. CAD was defined by $\geq$75% narrowing in one or more coronary arteries or clinical history of myocardial infarction or coronary artery bypass surgery or percutaneous coronary intervention. Of the included patients, whether the HF episode met Framingham criteria was reviewed by two investigators

* M. Imazu and H. Takahama contributed equally to this work.
Address for reprint requests and other correspondence: M. Kitakaze, National Cerebral and Cardiovascular Center, 5-7-1 Fujishirodai, Suita, Osaka 565-8565, Japan (e-mail: kitakaze@zf6.so-net.ne.jp).

0363-6135/14 Copyright © 2014 the American Physiological Society

(M. Imazu and H. Takahama) via medical records and confirmed that all patients met the criteria. Patients with cardiomyopathy underwent either myocardial biopsy or cardiac MRI for diagnosis. Diagnosis for cardiomyopathy was based on the definition of the World Health Organization/International Society and Federation Cardiology Task Force (23).

Biomarker measurements. Patients underwent a blood test for measurements of serum levels of FGF23, creatinine, calcium, phosphate, intact parathoroid hormone, troponin T, IL-6, TNF-α, plasma renin activity, and plasma levels of aldosterone in the present study before being discharged from the hospital. Blood sampled from the patients was placed in tubes with EDTA, and the serum was separated and frozen in plastic tubes at −80°C until analysis. The serum FGF23 level was measured with a chemiluminescence enzyme immunoassay (Kyowa Medex, Tokyo, Japan) as previously described (26). Both serum concentrations of IL-6 and TNF-α were measured with immu-

Table 1. *Baseline characteristics in NICD patients*

Characteristics	Below Median Group	Above Median Group	*P* Value
n	78	78	
Demographic data			
Age, yr	66 (IQR: 55–74)	57 (IQR: 43–69)	0.011
Women/men, %	60/40	40/60	0.010
New York Heart Association class III-IV, %	33	53	0.015
History			
HF hospitalization, %	23	60	<0.0001
Hypertension, %	50	37	0.106
Diabetes mellitus, %	21	27	0.324
Stroke, %	12	10	0.797
Atrial fibrillation, %	22	40	0.015
Etiology of NICD			<0.0001
Primary cardiomyopathy, *n*	19	38	0.235
Idiopathic dilated cardiomyopathy, *n*	9	24	
Hypertrophic cardiomyopathy, *n*	9	14	
Arrhythmogenic right ventricular cardiomyopathy, *n*	1	0	
Secondary cardiomyopathy, *n*	5	11	0.036
Amyloidosis, *n*	0	4	
Myocarditis, *n*	3	1	
Cardiac sarcoidosis, *n*	1	0	
Other, *n*	1	6	
Valvular disease, *n*	51	21	0.070
Aortic stenosis, *n*	21	4	
Aortic regurgitation, *n*	7	1	
Mitral stenosis, *n*	6	1	
Mitral regurgitation, *n*	10	8	
Tricuspid regurgitation, *n*	0	1	
Postvalve replacement, *n*	7	6	
Hypertensive heart disease with HF, *n*	3	8	
Physical findings			
Systolic blood pressure, mmHg	116 (IQR: 107–126)	104 (IQR: 93–118)	<0.0001
Heart rate, beats/min	65 (IQR: 58–76)	70 (IQR: 62–77)	0.081
Body mass index, kg/m^2	22.5 (IQR: 20.0–25.7)	22.1 (IQR: 19.9–25.3)	0.970
Medications			
β-Blockers, %	41	69	0.0004
Angiotensin-converting enzyme inhibitors or angiotensin II receptor blockers, %	46	64	0.024
Loop diuretics, %	22	62	<0.0001
Aldosterone antagonists, %	9	58	<0.0001
Statins, %	32	23	0.210
Laboratory data			
Phosphate, mg/dl	3.6 (IQR: 3.2–3.9)	3.7 (IQR: 3.3–4.1)	0.258
Intact parathyroid hormone, pg/dl	52 (IQR: 40–68)	56 (IQR: 41–80)	0.137
eGFR, ml·min^{-1}·1.73 m^{-2}	73 (IQR: 63–83)	69 (IQR: 55–80)	0.060
Troponin T, ng/ml	0.010 (IQR: 0.008–0.014)	0.015 (IQR: 0.009–0.023)	0.027
TNF-α, pg/ml	0.81 (IQR: 0.40–1.61)	1.36 (IQR: 0.85–2.05)	0.008
IL-6, pg/ml	1.51 (IQR: 0.92–2.66)	2.16 (IQR:1.29–3.19)	0.024
Plasma renin activity, ng·ml^{-1}·h^{-1}	1.4 (IQR: 0.4–3.8)	6.5 (IQR: 1.2–13.6)	0.0003
Plasma aldosterone concentration, ng/dl	12.6 (IQR: 8.5–16.3)	14.4 (IQR: 8.7–29.9)	0.032
Brain natriuretic peptide, pg/ml	81 (IQR: 41–162)	154 (IQR: 55–289)	0.007
TmP/GFR, mg/dl	3.29 (IQR: 2.90–3.55)	3.19 (IQR: 2.66–3.81)	0.797
FGF23, pg/ml	31.1 (IQR: 27.6–35.3)	51.3 (IQR: 43.2–61.5)	
Echocardiography data			
LVEDV index, ml/m^2	103 (IQR: 84–139)	128 (IQR: 90–165)	0.098
LVEF, %	63 (IQR: 45–68)	38 (IQR: 23–60)	<0.0001
Relative wall thickness	0.37 (IQR: 0.29–0.48)	0.33 (IQR: 0.25–0.41)	0.101
Left atrial volume index, ml/m^2	51 (IQR: 38–69)	57 (IQR: 49–71)	0.109

Values are numbers of patients (*n*), medians with interquartile ranges (IQRs), or percentages. The below median group comprised patients with a less than median value of serum fibroblast growth factor (FGF)23 level (39.1 pg/ml); the above median group comprised patients with a greater than median value of serum FGF23 level. NICD, nonischemic cardiac disease; HF, heart failure; eGFR, estimated glomerular filtration rate (eGFR); TmP/GFR, tubular maximal reabsorption rate of phosphate to GFR; LVEDV, left ventricular (LV) end-diastolic volume; LVEF, LV ejection fraction.

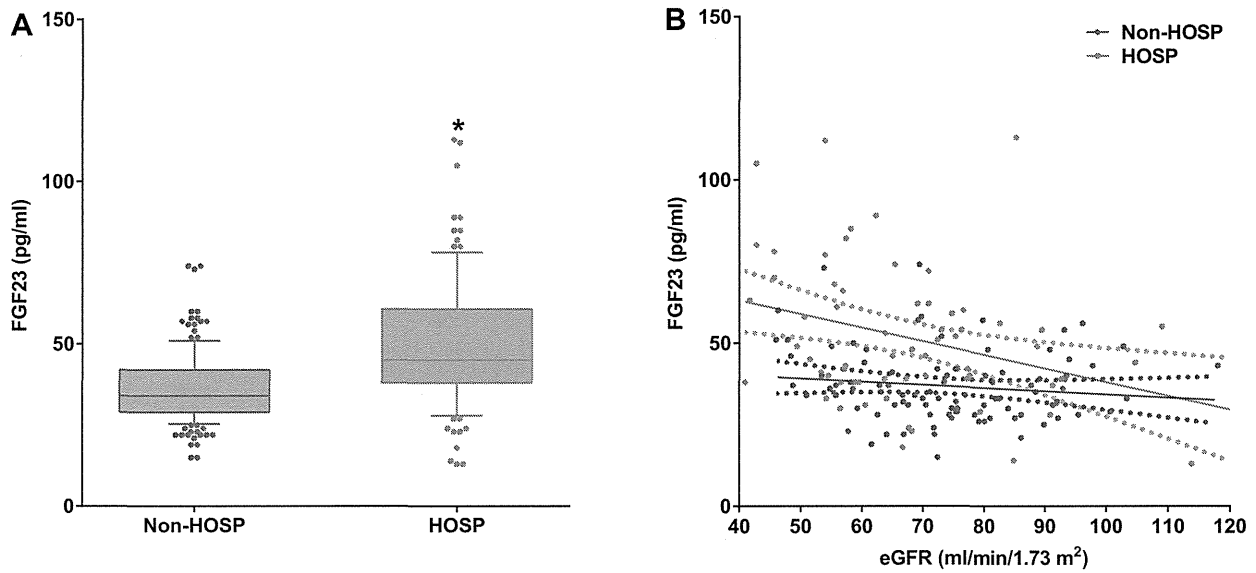

Fig. 1. Serum fibroblast growth factor (FGF)23 levels in patients with nonischemic cardiac disease (NICD). *A*: serum FGF23 levels in NICD patients. Red and blue squares show patients with a history of heart failure hospitalization (HOSP group) and without any history of HF hospitalization (non-HOSP group), respectively. $*P < 0.0001$, non-HOSP group vs. HOSP group. Values are shown as medians and 5–95% distribution. *B*: relationships between estimated glomerular filtration rate (eGFR) and serum FGF23 levels in NICD patients with and without a history of heart failure hospitalization. Graphs indicate the correlations between serum FGF23 levels and eGFR. Red and blue plots and lines show patients in the HOSP and non-HOSP groups, respectively. There was no difference in the relationship between eGFR and serum FGF23 levels in the non-HOSP group ($r = 0.129$, $P = 0.224$). In contrast, a steeper relationship between eGFR and serum FGF23 levels was found in patients in the HOSP group ($r = 0.342$, $P = 0.005$ in the HOSP group, group difference, $P = 0.042$).

noassays (R&D Systems). The plasma intact parathoroid hormone level was measured by an electrochemiluminescence immunoassay (Roche Diagnostics, Tokyo, Japan). eGFR (in $ml \cdot min^{-1} \cdot 1.73\ m^{-2}$) was calculated according to the following published equation for Japanese individuals: $194 \times \text{serum creatinine}^{-1.094} \times \text{age}^{-0.287}$ ($\times 0.739$ for women) (18). Both plasma renin activity and aldosterone concentration were measured by radioimmunoassays (Fujirebio, Tokyo, Japan). Urinary creatinine and phosphate concentrations were obtained via medical records. As previously described (2), the tubular reabsorption of phosphate (TRP) was calculated using the following equation: $1 - (U_P/P_P) \times (P_{Cr}/U_{Cr})$, where U_P and P_P are urine and plasma phosphate concentrations, respectively, and P_{Cr} and U_{Cr} are urine and plasma creatinine concentrations, respectively. The renal tubular maximum reabsorption rate of phosphate to GFR (TmP/GFR) was calculated according to the following equation: $TRP \times P_P$ (if $TRP \leq 0.86$) or $0.3 \times TRP/[1 - (0.8 \times TRP)] \times P_P$ (if $TRP > 0.86$).

Echocardiography. We retrospectively reviewed the data of echocardiography of the enrolled patients via their medical records. Left ventricular (LV) dimensions, left atrium volume, and wall thickness were measured according to American Society of Echocardiography guidelines (16). LV ejection fraction (LVEF) was measured using the Simpson biplane method or the semiquantitative two-dimensional visual estimate method as previously described (22). LV end-diastolic volume and mass were calculated using the Teichholz and Devereux formula (3, 27), respectively.

Right heart catheterization. The indication of right heart catheterization (RHC) was determined by the need of disease managements for an assessment for the HF severity for hospitalized patients. We collected the data from all enrolled patients who underwent RHC. Standard RHC was performed using a Swan-Ganz catheter (Goodman, Tokyo, Japan). Cardiac output was calculated with the direct Fick method as O_2 consumption divided by the arteriovenous O_2 difference, as previously described (15). Briefly, O_2 consumption was obtained by a respiratory gas analyzer (Aeromonitor AE-300S, Minato Medical Science, Osaka, Japan). Levels of hemoglobin, O_2 saturation, and Po_2 (arterial and venous Po_2) were measured by a blood gas analyzer (OSM3, Radiometer, Copenhagen, Denmark). Blood from a vein was sampled from the pulmonary artery.

Clinical outcomes. After the enrollment in this study, we investigated cardiovascular death, heart transplantation, implantation of a LV assist device, and rehospitalization for HF over 1 yr through medical chart review or a letter. Cardiovascular events were defined as a composite of cardiovascular death, implantation of a LV assist device, or rehospitalization for HF.

Ethics. Written informed consent was obtained from all subjects. This study was approved by our institutional ethics committee and was conducted in accordance with the Declaration of Helsinki.

Statistical analysis. Data are expressed as medians and interquartile ranges (IQRs). Between-group differences were compared with a χ^2-test for categorical variables. Student's *t*-test (normalized distributed data) or Wilcoxon's rank sum test (non-normalized distributed data) was used for the comparison of continuous variables between two groups. Pearson's correlation coefficient analysis or Spearman's rank correlation coefficient analysis and linear regression were used to assess the relationships between FGF23 levels and other variables. The multiple linear regression model was used to test multiple covariates. All variables with $P < 0.10$ in univariate analysis were selected and performed into the multivariable models. All tests were

Table 2. *Comparison of serum FGF23 levels in non-HF and HF patients*

Nonhospitalized group versus hospitalized group	Adjusted Mean Difference	95% Confidence Interval	*P* Value
Model 1	−7.260	−9.877, −4.642	<0.0001
Model 2	−6.190	−8.802, −3.578	<0.0001
Model 3	−3.989	−6.771, −1.206	0.005

Model 1 was adjusted for age and sex, *model 2* was adjusted for age, sex, and eGFR, and *model 3* was adjusted for age, sex, eGFR, and use of loop diuretics (yes = 1).

Table 3. *Univariate and multivariate analyses of serum FGF23 levels in laboratory data*

Variables	Univariate Analysis			Multivariate Analysis		
	Regression coefficient, pg/ml	95% confidence interval	*P* value	Regression coefficient, pg/ml	95% confidence interval	*P* value
eGFR	−0.329	−0.495, −0.163	0.0001	0.237	−0.510, 0.037	0.089
Troponin T	235.8	2.741, 468.9	0.047	70.40	−185.9, 326.7	0.587
TNF-α	2.227	0.260, 4.194	0.027	2.715	−0.538, 5.968	0.101
IL-6	0.628	−0.580, 1.837	0.306			
White blood cell count	0.0003	−0.0013, 0.0019	0.747			
C-reactive protein	2.579	−5.967, 11.13	0.552			
Plasma aldosterone concentration	0.384	0.194, 0.573	0.0001	0.345	0.122, 0.567	0.003

n = 156 patients total. In the multivariate model, age and sex were adjusted.

two-tailed, and P values of <0.05 were considered significant. These analyses were performed with JMP 10 (SAS Institute, Cary, NC).

RESULTS

Relationship between clinical features of NICD-induced HF patients and serum FGF23 levels. We excluded 25 CAD patients from this study according to the aim of this study and the criteria. Of the remaining 156 patients, we divided the patients into above and below median FGF23 levels (39.1 pg/ml), as shown in Table 1 (above or below median groups). Between these two groups, higher prevalence of New York Heart Association (NYHA) class III-IV at admission (53% vs. 33%, P = 0.015) and HF hospitalization (60% vs. 23%, P < 0.0001) were frequently observed in the above median group. We also observed a higher proportion of patients with cardiomyopathy (62% vs. 28%, P < 0.0001) and atrial fibrillation (40% vs. 22%, P = 0.015) and a lower systolic blood pressure [104 (IQR: 93–118) vs. 116 (IQR: 107–126) mmHg, P < 0.0001] in the above median group. Loop diuretics were frequently used in the above median group compared with the below median group (62% vs. 22%, P < 0.0001). Aldosterone antagonists were frequently used in the above median group compared with the below median group (58% vs. 9%, P < 0.0001). eGFR was on the statistical border between the two groups (P = 0.060). Blood levels of troponin T, TNF-α, IL-6, and aldosterone were higher in the above median group than in the below median group (Table 1). Echocardiography revealed a lower degree of LVEF in the above median group [38 (IQR: 23–60)% vs. 63 (45–68)%, P < 0.0001]. There were no significant differences regarding the LV end-diastolic volume index, relative wall thickness, and left atrial volume index between the groups. The subtype of cardiac disease is shown in Table. 1. There was no patient with a history of kidney transplant or kidney disease. TmP/GFR was measured in 104 patients, and we found no differences between the above and below median FGF23 groups (Table 1). In the analysis between serum FGF23 levels and physiological variables, serum FGF23 levels were related to mean blood pressure (r = −0.281, P = 0.003) but were not related to heart rate (r = 0.090, P = 0.267) and body mass index (r = −0.017, P = 0.830).

Serum FGF23 levels in NICD-induced HF patients. We investigated serum FGF23 levels in patients with or without a history of HF hospitalization (hospitalized or nonhospitalized groups, respectively). Serum FGF23 levels were higher in the hospitalized group compared with the nonhospitalized group [34.7 (IQR: 29.6–42.4) vs. 46.8 (IQR: 38.8–62.7), P < 0.0001; Fig. 1*A*]. Figure 1*B* shows the relationship between eGFR and FGF23 levels in the hospitalized and nonhospitalized groups. There were no differences in the relationship between eGFR and serum FGF23 levels in the nonhospitalized group (r = 0.129, P = 0.224). In contrast, as eGFR decreased, serum FGF23 levels were elevated at a higher rate for the hospitalized group than for the nonhospitalized group (r = 0.342, P = 0.005 in the hospitalized group, group difference, P = 0.042). Table 2 shows the multivariate linear model of serum FGF23 levels in these groups. Serum FGF23 levels were higher in the hospitalized group even after adjustments of age, sex, eGFR, and the use of loop diuretics. TmP/GFR did not differ between the hospitalized and nonhospitalized groups.

Predictor of serum FGF23 levels in NICD-induced HF patients. Table 3 shows the relationships between serum FGF23 levels and other laboratory markers. eGFR, troponin T, TNF-α, and plasma aldosterone concentration were related to FGF23 levels in the univariate analysis. In the multivariate analysis, plasma aldosterone concentration was the only factor related to serum FGF23 levels (P = 0.003). Table 4 shows the relationship of serum FGF23 levels with ventricular structural and functional values as assessed by echocardiography. In the multivariate analysis, LVEF was the only factor related to serum FGF23 levels (P = 0.020). Table 5 shows the multivariate analysis for the relationship of serum FGF23 levels with history of HF hospitalization, plasma aldosterone concentration, LVEF, and use of diuretics after adjusting for age, sex,

Table 4. *Univariate and multivariate analyses of FGF23 in echocardiography data*

Variables	Univariate Analysis			Multivariate Analysis		
	Regression coefficient, pg/ml	95% confidence interval	*P* value	Regression coefficient, pg/ml	95% confidence interval	*P* value
LVEDV index	0.083	0.030, 0.136	0.003	0.032	−0.054, 0.118	0.462
LVEF	−0.348	−0.500, −0.197	<0.0001	−0.251	−0.461, −0.040	0.020
Relative wall thickness	−15.66	−33.82, 2.496	0.090	11.35	−11.84, 34.54	0.334

In the multivariate model, age, sex, and eGFR were adjusted.

Table 5. *Multivariate analysis of FGF23*

Variables	Multivariate Analysis		
	Regression coefficient, pg/ml	95% confidence interval	*P* value
History of HF hospitalization	−4.330	−8.250, −0.411	0.031
Plasma aldosterone concentration	0.236	0.041, 0.431	0.018
LVEF	−0.141	−0.344, 0.063	0.174
Use of loop diuretics	−3.042	−0.629, 0.201	0.066

n = 156 patients total. In the multivariate model, age, sex, and eGFR were adjusted.

and eGFR. The history of HF hospitalization (P = 0.031) and plasma aldosterone concentration (P = 0.018) were independently related to serum FGF23 levels in this model.

Relationships of systolic function with serum FGF23 levels and other laboratory markers. To test the correlation of LVEF with the laboratory data, including serum FGF23 levels, we performed multivariate regression analyses. The results are shown in Table 6. In the multivariate model, after adjusting for age and sex, serum FGF23 levels were correlated with LVEF (P = 0.001), whereas no relationships with LVEF were found in eGFR, TNF-α, and plasma aldosterone concentration.

Relationship between serum FGF23 levels and the hemodynamic state. Table 7 shows the central hemodynamic data obtained through RHC in 127 patients. In the above median FGF23 group, the cardiac index was significantly lower compared with the below median group [2.4 (IQR: 1.9–2.7) vs. 2.7 (IQR: 2.4–3.1) $l \cdot min^{-1} \cdot m^{-2}$, P = 0.001]. Table 8 shows the relationship between serum FGF23 levels and hemodynamic values as assessed by RHC. In the multivariate analysis, the cardiac index was the only factor related to serum FGF23 levels (P = 0.018).

Predictive value of serum FGF23 levels for clinical outcomes. During the 1-yr followup term, cardiovascular events occurred in 15 patients (cardiac death: 1 patient, implantation of a LV assist device: 2 patients, and rehospitalization for HF: 12 patients). Kaplan-Meier analysis showed that the frequency of cardiovascular events were higher in the above median FGF23 group than in the below median FGF23 group (P = 0.005; Fig. 2). Even after adjustments for age, sex, and eGFR, the predictability of serum FGF23 levels for cardiovascular events persisted (Table 9).

DISCUSSION

The present study showed that serum FGF23 levels were elevated in NICD patients who had a HF hospitalization history compared with patients without any HF hospitalization history. Although it is known that the circulating FGF23 level is influenced by other variables, such as renal function (28), we prospectively measured serum FGF23 levels in patients without advanced renal impairment and confirmed the pathophysiological importance of serum FGF23 levels in patients with HF history even in the early stages of CKD. The multivariate analysis in the present study revealed that HF hospitalization history was the strongest predictor for the elevation of serum FGF23 levels in NICD. The present study also revealed that serum FGF23 levels are tightly related to plasma aldosterone levels and that systolic dysfunction and low cardiac output are tightly related to serum FGF23 levels. Taken together, we raise the possibility that such pathogenesis and risk factors for the development of HF are the determinants of serum FGF23 levels in NICD patients. In addition, among the neurohormonal parameters measured in the present study, an elevated serum FGF23 level was the only factor to predict a declining LVEF level. Furthermore, even after adjustments for age, sex, and eGFR, the serum FGF23 level was a strong predictor for future cardiovascular events in the present study. Consistent with previous studies reporting that circulating FGF23 levels can affect cardiac structure and function, our findings suggest that the progression of HF contributes to the elevation of circulating FGF23 levels, which leads to further myocardial dysfunction, potentially creating a vicious cycle.

Serum FGF23 levels in NICD-induced HF patients. There has been less evidence of circulating FGF23 levels in HF patients with preserved renal function. This study confirmed that in NICD patients, even in the early stages of CKD, serum FGF23 levels are elevated in those with a history of HF hospitalization compared with those without HF hospitalization history (Fig. 1). We also confirmed higher serum FGF23 levels in HF patients even accounting for age, sex, eGFR, and the use of diuretics (Table 2). The determinants of serum FGF23 levels have not been completely clarified in previous studies of HF patients. Our findings suggest that NICD-induced HF hospitalization itself is one of the strong determinants of serum FGF23 levels even in a population with relatively preserved renal function. Figure 1*B* shows that there was a steeper negative slope between serum FGF23 levels and eGFR in the hospitalized group compared with the nonhospitalized group, suggesting that serum FGF23 levels are elevated in HF patients even in the early stages of CKD. Although the responsible factors for the elevation of serum FGF23 levels in HF patients have been remained uncertain in previous studies, we identified high plasma aldosterone concentration (Table 3), low LVEF (Table 4), and low cardiac index (Table 8) as predictors for the elevation of serum FGF23 levels even after accounting for eGFR. Whether low cardiac output itself independently contributes to the elevation of serum FGF23 levels from renal function still remains controversial. Interestingly, we also found that in the above median FGF23 group, the percentage of patients who took a loop diuretics was higher than in the below median group ($P < 0.0001$; Table 1), and we can raise the possibility that decreased renal perfusion by diuretics affects serum FGF23 levels. Consisted with these findings, a previous study (9) has suggested the relationship between the use of diuretics and circulating FGF23 levels. As a speculation, we also suggest that decreasing renal perfusion

Table 6. *Multivariate linear model of LVEF in laboratory data*

Variables	Multivariate Analysis		
	Regression coefficient, pg/ml	95% confidence interval	*P* value
eGFR	0.116	−0.109, 0.341	0.308
TNF-α	0.664	−1.308, 2.635	0.506
Plasma aldosterone concentration	−0.145	−0.359, 0.070	0.184
FGF23	−0.340	−0.531, −0.150	0.001

In the multivariate model, age and sex were adjusted.

Table 7. *Right heart catheterization data*

	Below Median Group	Above Median Group	*P* Value
Right atrial pressure, mmHg	4 (IQR: 2–5)	4 (IQR: 2–5)	0.553
Mean pulmonary artery pressure, mmHg	17 (IQR: 14–20)	18 (IQR: 13–25)	0.207
Pulmonary capillary wedge pressure, mmHg	10 (IQR: 7–12)	11 (IQR: 6–17)	0.345
Cardiac index, $l \cdot min^{-1} \cdot m^{-2}$	2.7 (IQR: 2.4–3.1)	2.4 (IQR: 1.9–2.7)	0.001

Values are medians with IQRs; n = 67 patients in the below median group and 60 patients in the above median group.

induced by a low cardiac output state is one of the key factors affecting serum FGF23 levels. Although eGFR in the present study was relatively preserved (median eGFR: 73 and 69 $ml \cdot min^{-1} \cdot m^{-2}$ in below and above median FGF23 groups, respectively), the findings of steeper correlation between serum FGF23 levels and eGFR in the hospitalized group also support the hypothesis. Our findings also suggest a positive relationship between serum FGF23 levels and neurohormone activation or inflammatory markers, such as TNF-α. These findings are consistent with those of previous study (1) with the respect to the relationship between inflammatory markers and FGF23 levels in CKD patients, suggesting that inflammation is associated with an elevation of circulating FGF23 levels in HF patients. Our findings also demonstrate that there was no longer a relationship between TNF-α and serum FGF23 levels in multivariate analysis (Table 3), with a possible explanation that there might be an interplay between several factors, such as neurohormonal activation and inflammation, for elevating serum FGF23 levels. Interestingly, a more recent study (17) has raised the possibility of endogenous Klotho expression in arteries. Inflammatory cytokines, such as TNF-α, downregulate Klotho expression in the kidney through NF-κB (19) or suppress the expression of both Klotho and FGF receptor in an in vitro study (17). It is worth considering the interplay among neurohormonal activation, inflammatory cytokines, vascular Klotho, and circulating FGF23 levels in patients with HF, and further investigation will be necessary to solve it. Taken together, our results could not explain the mechanism of elevating serum FGF23 levels by a single factor. Indeed, in multivariate analysis (Table 5), LVEF was not correlated with serum FGF23 levels. In addition, we found that aldosterone antagonists were frequently used in the above median group compared with the below median group (58% vs. 9%, $P < 0.001$). This might also influence the higher plasma aldosterone concentration in the above median group. We suggest that such complex interaction or underlying conditions predisposing to the development of HF contribute to the elevation of serum FGF23 levels in NICD patients.

Between the hospitalized and nonhospitalized groups, the differences of serum FGF23 levels were statistically significant, but small. Because of such low circulating levels of FGF23, it is worth to consider whether FGF23 is a "pure" endocrine factor to play a role on cardiac remodeling. Interestingly, some studies (5, 14) have suggested the presence of circulating progenitor cells, which are capable of differentiating into osteoblasts. These findings facilitated us to the further investigation to elucidate the relationship between circulating progenitor cells and serum FGF23 levels. The relationships between such a low level of circulating FGF23 and FGF23 signaling in cardiomyocytes or the endothelium and the interaction with vascular Klotho have also remained uncertain; further investigation will be needed to determine their relationships.

In addition, a clinical study (7) has suggested that circulating FGF23 levels are associated with the degree of LV hypertrophy in patients with CKD. In this study, we determined that serum FGF23 levels were significantly correlated with LV systolic function and cardiac output but were not related to the degree of cardiac hypertrophy. Because the stages of CKD in our patients were relatively early, these differences from previous studies also raise the possibilities that CKD stages and serum FGF23 levels are correlated with the cardiac phenotype. In accordance with this finding, the phosphate reabsorption, as indicated by TmP/GFR, did not differ between the above and below median groups in the present study. This finding suggests that serum FGF23 levels were relatively lower than advanced CKD patients because of our focus on NICD patients with early stages of CKD.

Limitations. We acknowledge that our study has some limitations that merit noting. First, this study was a single-center study, which poses a possible bias risk regarding HF severity and etiologies. Second, although differences in the etiologies of NICD were found between the below and above median FGF23 groups, the present study included valvular disease patients with milder HF symptoms, who hospitalized for an elective catheter test. These variances influence the differences of HF etiologies between the below and above median FGF23 groups. Age differences were observed between the above and below median FGF23 groups. Even after accounting for the age differences in the multivariate models, we confirmed that

Table 8. *Univariate and multivariate analyses of FGF23 in right heart catheterization data*

	Univariate Analysis			Multivariate Analysis		
Variables	Regression coefficient, pg/ml	95% confidence interval	*P* value	Regression coefficient, pg/ml	95% confidence interval	*P* value
Right atrial pressure	1.547	0.494, 2.601	0.004	0.612	−0.594, 1.820	0.317
Mean pulmonary artery pressure	0.503	0.120, 0.885	0.010	0.501	−0.095, 1.097	0.098
Pulmonary capillary wedge pressure	0.612	0.083, 1.142	0.024	−0.551	−1.450, 0.347	0.227
Cardiac index	−6.697	−10.73, −2.669	0.001	−4.532	−0.894, −0.126	0.044

n = 127 patients total. In the multivariate model, age, sex, and eGFR were adjusted.

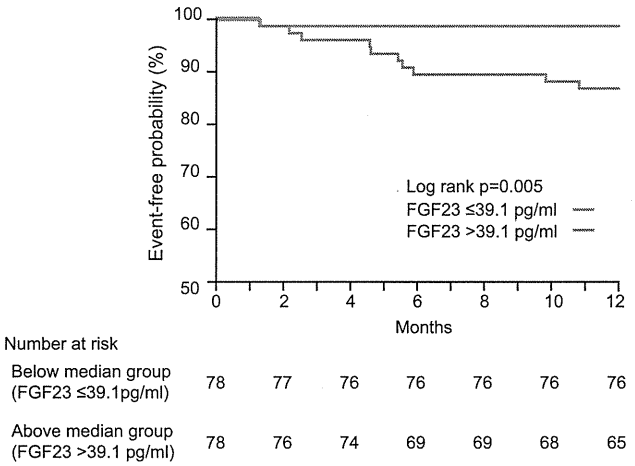

Fig. 2. Kaplan-Meier analysis for cardiovascular events in the below and above median FGF23 groups. Red and blue lines show the below and above median FGF23 groups, respectively. Kaplan-Meier analysis showed that the frequency of cardiovascular events was higher in the above median FGF23 group than in the below median FGF23 group (P = 0.005).

serum FGF23 levels were higher in patients with HF hospitalization history. We also demonstrated the predictive value of serum FGF23 levels for clinical outcome even after accounting for age differences in the multivariate models. There were a few patients with extreme outlier values, as shown in Fig. 1*B*. No confounding factor for the elevation of serum FGF23 levels, such as a past history of bone metabolic disease, was found in patients. However, after the exclusion of patients with outlier values, a similar tendency was found (r = 0.411, P = 0.0008). Urine tests were not performed in all enrolled patients, because the results of urine tests were taken from a part of clinical routine tests. Nevertheless, the subanalysis for TmP/GFR might provide us some information regarding relative levels of serum FGF23 levels.

Conclusions. Serum FGF23 levels were elevated in NICD patients with a history of HF hospitalization even though their renal function was relatively preserved. We demonstrated that the underlying substrates of HF, such as cardiac dysfunction and neurohormonal activation, are associated with an elevation of serum FGF23 levels in our patients and suggest that the progression of HF itself contributes to the elevation of circulating FGF23 levels even in early CKD, which leads to further myocardial dysfunction, potentially creating a vicious cycle.

ACKNOWLEDGMENTS

The authors thank Akiko Ogai for assistance with the centrifugation of blood samples and Toshimitsu Hamasaki for advice about the statistics.

GRANTS

This work was supported by Japanese Ministry of Health, Labor, and Welfare Grant-In-Aid H23-Nanchi-Ippan-22 (to M. Kitakaze).

DISCLOSURES

No conflicts of interest, financial or otherwise, are declared by the author(s).

AUTHOR CONTRIBUTIONS

Author contributions: M.I., H.T., A.F., Y.S., T.O., T.H., and M.A. analyzed data; M.I., H.T., A.F., Y.S., T.O., T.H., and M.A. interpreted results of experiments; M.I. and H.T. prepared figures; M.I., H.T., and M.K. drafted manuscript; H.T. and M.K. conception and design of research; H.A., T.H., H.K., T.A., and M.K. edited and revised manuscript; M.K. approved final version of manuscript.

REFERENCES

1. **ADHR Consortium.** Autosomal dominant hypophosphataemic rickets is associated with mutations in FGF23. *Nat Genet* 26: 345–348, 2000.
2. **Barth JH, Jones RG, Payne RB.** Calculation of renal tubular reabsorption of phosphate: the algorithm performs better than the nomogram. *Ann Clin Biochem* 37: 79–81, 2000.
3. **Devereux RB, Alonso DR, Lutas EM, Gottlieb GJ, Campo E, Sachs I, Reichek N.** Echocardiographic assessment of left ventricular hypertrophy: comparison to necropsy findings. *Am J Cardiol* 57: 450–458, 1986.
4. **Faul C, Amaral AP, Oskouei B, Hu MC, Sloan A, Isakova T, Gutierrez OM, Aguillon-Prada R, Lincoln J, Hare JM, Mundel P, Morales A, Scialla J, Fischer M, Soliman EZ, Chen J, Go AS, Rosas SE, Nessel L, Townsend RR, Feldman HI, St John Sutton M, Ojo A, Gadegbeku C, Di Marco GS, Reuter S, Kentrup D, Tiemann K, Brand M, Hill JA, Moe OW, Kuro OM, Kusek JW, Keane MG, Wolf M.** FGF23 induces left ventricular hypertrophy. *J Clin Invest* 121: 4393–4408, 2011.
5. **Gossl M, Khosla S, Zhang X, Higano N, Jordan KL, Loeffler D, Enriquez-Sarano M, Lennon RJ, McGregor U, Lerman LO, Lerman A.** Role of circulating osteogenic progenitor cells in calcific aortic stenosis. *J Am Coll Cardiol* 60: 1945–1953, 2012.
6. **Gutierrez O, Isakova T, Rhee E, Shah A, Holmes J, Collerone G, Juppner H, Wolf M.** Fibroblast growth factor-23 mitigates hyperphosphatemia but accentuates calcitriol deficiency in chronic kidney disease. *J Am Soc Nephrol* 16: 2205–2215, 2005.
7. **Gutierrez OM, Januzzi JL, Isakova T, Laliberte K, Smith K, Collerone G, Sarwar A, Hoffmann U, Coglianese E, Christenson R, Wang TJ, deFilippi C, Wolf M.** Fibroblast growth factor 23 and left ventricular hypertrophy in chronic kidney disease. *Circulation* 119: 2545–2552, 2009.
8. **Gutierrez OM, Mannstadt M, Isakova T, Rauh-Hain JA, Tamez H, Shah A, Smith K, Lee H, Thadhani R, Juppner H, Wolf M.** Fibroblast growth factor 23 and mortality among patients undergoing hemodialysis. *N Engl J Med* 359: 584–592, 2008.
9. **Isakova T, Houston J, Santacruz L, Schiavenato E, Somarriba G, Harmon WG, Lipshultz SE, Miller TL, Rusconi PG.** Associations between fibroblast growth factor 23 and cardiac characteristics in pediatric heart failure. *Pediatr Nephrol* 28: 2035–2042, 2013.
10. **Ix JH, Katz R, Kestenbaum BR, de Boer IH, Chonchol M, Mukamal KJ, Rifkin D, Siscovick DS, Sarnak MJ, Shlipak MG.** Fibroblast growth factor-23 and death, heart failure, and cardiovascular events in community-living individuals: CHS (Cardiovascular Health Study). *J Am Coll Cardiol* 60: 200–207, 2012.
11. **Jonsson KB, Zahradnik R, Larsson T, White KE, Sugimoto T, Imanishi Y, Yamamoto T, Hampson G, Koshiyama H, Ljunggren O, Oba K, Yang IM, Miyauchi A, Econs MJ, Lavigne J, Juppner H.** Fibroblast growth factor 23 in oncogenic osteomalacia and X-linked hypophosphatemia. *N Engl J Med* 348: 1656–1663, 2003.
12. **Kendrick J, Cheung AK, Kaufman JS, Greene T, Roberts WL, Smits G, Chonchol M.** FGF-23 associates with death, cardiovascular events, and initiation of chronic dialysis. *J Am Soc Nephrol* 22: 1913–1922, 2011.
13. **Kestenbaum B, Sampson JN, Rudser KD, Patterson DJ, Seliger SL, Young B, Sherrard DJ, Andress DL.** Serum phosphate levels and mortality risk among people with chronic kidney disease. *J Am Soc Nephrol* 16: 520–528, 2005.
14. **Kuroda R, Matsumoto T, Kawakami Y, Fukui T, Mifune Y, Kurosaka M.** Clinical impact of circulating CD34-positive cells on bone regeneration and healing. *Tissue Eng Part B Rev* 20: 190–199, 2014.

Table 9. *Predictive value of serum FGF23 levels for cardiovascular events*

Above Median Value Versus Below Median Value	Hazard Ratios	95% Confidence Interval	*P* Value
Unadjusted	1.05	1.03, 1.07	<0.0001
Model 1	1.05	1.03, 1.08	<0.0001
Model 2	1.06	1.03, 1.09	<0.0001

Model 1 was adjusted for age and sex, and *model 2* was adjusted for age, sex, and eGFR.

15. **La Gerche A, Claessen G, Van de Bruaene A, Pattyn N, Van Cleemput J, Gewillig M, Bogaert J, Dymarkowski S, Claus P, Heidbuchel H.** Cardiac MRI: a new gold standard for ventricular volume quantification during high-intensity exercise. *Circ Cardiovasc Imaging* 6: 329–338, 2013.
16. **Lang RM, Bierig M, Devereux RB, Flachskampf FA, Foster E, Pellikka PA, Picard MH, Roman MJ, Seward J, Shanewise JS, Solomon SD, Spencer KT, Sutton MS, Stewart WJ.** Recommendations for chamber quantification: a report from the American Society of Echocardiography's Guidelines and Standards Committee and the Chamber Quantification Writing Group, developed in conjunction with the European Association of Echocardiography, a branch of the European Society of Cardiology. *J Am Soc Echocardiogr* 18: 1440–1463, 2005.
17. **Lim K, Lu TS, Molostvov G, Lee C, Lam FT, Zehnder D, Hsiao LL.** Vascular Klotho deficiency potentiates the development of human artery calcification and mediates resistance to fibroblast growth factor 23. *Circulation* 125: 2243–2255, 2012.
18. **Matsuo S, Imai E, Horio M, Yasuda Y, Tomita K, Nitta K, Yamagata K, Tomino Y, Yokoyama H, Hishida A.** Revised equations for estimated GFR from serum creatinine in Japan. *Am J Kidney Dis* 53: 982–992, 2009.
19. **Moreno JA, Izquierdo MC, Sanchez-Nino MD, Suarez-Alvarez B, Lopez-Larrea C, Jakubowski A, Blanco J, Ramirez R, Selgas R, Ruiz-Ortega M, Egido J, Ortiz A, Sanz AB.** The inflammatory cytokines TWEAK and TNFα reduce renal klotho expression through NFκB. *J Am Soc Nephrol* 22: 1315–1325, 2011.
20. **Plischke M, Neuhold S, Adlbrecht C, Bielesz B, Shayganfar S, Bieglmayer C, Szekeres T, Horl WH, Strunk G, Vavken P, Pacher R, Hulsmann M.** Inorganic phosphate and FGF-23 predict outcome in stable systolic heart failure. *Eur J Clin Invest* 42: 649–656, 2012.
21. **Razzaque MS.** The FGF23-Klotho axis: endocrine regulation of phosphate homeostasis. *Nat Rev Endocrinol* 5: 611–619, 2009.
22. **Redfield MM, Jacobsen SJ, Burnett JC, Jr., Mahoney DW, Bailey KR, Rodeheffer RJ.** Burden of systolic and diastolic ventricular dysfunction in the community: appreciating the scope of the heart failure epidemic. *JAMA* 289: 194–202, 2003.
23. **Richardson P, McKenna W, Bristow M, Maisch B, Mautner B, O'Connell J, Olsen E, Thiene G, Goodwin J, Gyarfas I, Martin I, Nordet P.** Report of the 1995 World Health Organization/International Society and Federation of Cardiology Task Force on the definition and classification of cardiomyopathies. *Circulation* 93: 841–842, 1996.
24. **Roos M, Lutz J, Salmhofer H, Luppa P, Knauss A, Braun S, Martinof S, Schomig A, Heemann U, Kastrati A, Hausleiter J.** Relation between plasma fibroblast growth factor-23, serum fetuin-A levels and coronary artery calcification evaluated by multislice computed tomography in patients with normal kidney function. *Clin Endocrinol (Oxf)* 68: 660–665, 2008.
25. **Seiler S, Cremers B, Rebling NM, Hornof F, Jeken J, Kersting S, Steimle C, Ege P, Fehrenz M, Rogacev KS, Scheller B, Bohm M, Fliser D, Heine GH.** The phosphatonin fibroblast growth factor 23 links calcium-phosphate metabolism with left-ventricular dysfunction and atrial fibrillation. *Eur Heart J* 32: 2688–2696, 2011.
26. **Shimizu Y, Fukumoto S, Fujita T.** Evaluation of a new automated chemiluminescence immunoassay for FGF23. *J Bone Miner Metab* 30: 217–221, 2012.
27. **Teichholz LE, Kreulen T, Herman MV, Gorlin R.** Problems in echocardiographic volume determinations: echocardiographic-angiographic correlations in the presence of absence of asynergy. *Am J Cardiol* 37: 7–11, 1976.
28. **Wolf M.** Forging forward with 10 burning questions on FGF23 in kidney disease. *J Am Soc Nephrol* 21: 1427–1435, 2010.

nature COMMUNICATIONS

ARTICLE

Received 16 Jul 2014 | Accepted 12 Dec 2014 | Published 30 Jan 2015

DOI: 10.1038/ncomms7137 OPEN

Augmented AMPK activity inhibits cell migration by phosphorylating the novel substrate Pdlim5

Yi Yan[1,*], Osamu Tsukamoto[1,*], Atsushi Nakano[2], Hisakazu Kato[1], Hidetaka Kioka[3], Noriaki Ito[3], Shuichiro Higo[3], Satoru Yamazaki[4], Yasunori Shintani[1], Ken Matsuoka[3], Yulin Liao[5], Hiroshi Asanuma[2], Masanori Asakura[2], Kazuaki Takafuji[6], Tetsuo Minamino[3], Yoshihiro Asano[3], Masafumi Kitakaze[2] & Seiji Takashima[1,7]

Augmented AMP-activated protein kinase (AMPK) activity inhibits cell migration, possibly contributing to the clinical benefits of chemical AMPK activators in preventing atherosclerosis, vascular remodelling and cancer metastasis. However, the underlying mechanisms remain largely unknown. Here we identify PDZ and LIM domain 5 (Pdlim5) as a novel AMPK substrate and show that it plays a critical role in the inhibition of cell migration. AMPK directly phosphorylates Pdlim5 at Ser177. Exogenous expression of phosphomimetic S177D-Pdlim5 inhibits cell migration and attenuates lamellipodia formation. Consistent with this observation, S177D-Pdlim5 suppresses Rac1 activity at the cell periphery and displaces the Arp2/3 complex from the leading edge. Notably, S177D-Pdlim5, but not WT-Pdlim5, attenuates the association with Rac1-specific guanine nucleotide exchange factors at the cell periphery. Taken together, our findings indicate that phosphorylation of Pdlim5 on Ser177 by AMPK mediates inhibition of cell migration by suppressing the Rac1-Arp2/3 signalling pathway.

[1] Department of Medical Biochemistry, Osaka University Graduate School of Medicine, 2-2 Yamadaoka, Suita, Osaka 565-0871, Japan. [2] Depertment of Clinical Research and Development, National Cerebral and Cardiovascular Center Research Institute, Suita, Osaka 565-8565, Japan. [3] Department of Cardiovascular Medicine, Osaka University Graduate School of Medicine, 2-2 Yamadaoka, Suita, Osaka 565-0871, Japan. [4] Department of Cell Biology, National Cerebral and Cardiovascular Center Research Institute, Suita, Osaka 565-8565, Japan. [5] Department of Cardiology, Nanfang Hospital, Southern Medical University, 1838 North Guangzhou Avenue, 510515 Guangzhou, China. [6] Center for Research Education, Osaka University Graduate School of Medicine, 2-2 Yamadaoka, Suita, Osaka 565-0871, Japan. [7] Japan Science and Technology Agency-Core Research for Evolutional Science and Technology (CREST), Kawaguchi 332-0012, Japan. * These authors contributed equally to this work.. Correspondence and requests for materials should be addressed to O.T. (email: tsuka@medbio.med.osaka-u.ac.jp).

© 2015 Macmillan Publishers Limited. All rights reserved.

AMP-activated protein kinase (AMPK), generally considered an energy sensor kinase, requires AMP for activation[1]. Recently, a growing body of evidence has revealed that AMPK also plays a key role in the establishment of cell polarity and motility[2,3]. We previously reported that AMPK regulates cell migration by controlling microtubule dynamics through phosphorylation of a cytoplasmic linker protein-170 (CLIP-170)[4]. Moreover, recent studies have implicated AMPK in the regulation of actin cytoskeleton dynamics and reorganization at the plasma membrane[5,6]. Thus, AMPK is predicted to regulate cell migration by controlling both microtubule and actin-filament dynamics.

Cell migration is a physically integrated molecular process that begins with dynamic polarization and formation of lamellipodia, membrane protrusions at the leading edges of cells[7]. Rac1, a Rho-family small GTPase, is a key upstream regulator of actin dynamics and organization, and is necessary for the formation of persistent lamellipodia leading to directional cell migration[8,9]. Once Rac1 is activated by guanine nucleotide exchange factors (GEFs) at the leading edge, the activated form (GTP-bound Rac1) recruits a complex containing its downstream effector Wiskott–Aldrich Syndrome protein family verprolin homologous to the plasma membrane, leading in turn to activation of the actin-related protein 2/3 (Arp2/3) complex[10,11]. Activated Arp2/3 complex functions as an efficient nucleator[10,11] to organize the branched actin-filament network involved in formation of lamellipodia, a critical step in cell migration.

Some drugs in clinical use have the potential to indirectly activate AMPK. These compounds have been convincingly shown to prevent atherosclerosis, vascular remodelling, and tumour invasion and metastasis[12–17], processes in which dysregulated cell migration contributes to the development and progression of diseases. Accordingly, the clinically beneficial effects of chemical AMPK activators can be partially attributed to inhibition of cell migration via augmentation of AMPK activity. However, the mechanisms by which augmented AMPK activity inhibits cell migration remain largely unknown.

In this study, we identified PDZ and LIM domain 5 (Pdlim5)[18] as a novel substrate of AMPK; Pdlim5 is directly phosphorylated by AMPK at Ser177. This phosphorylation results in displacement of Rho GEF 6 (Arhgef6), a Rac1/Cdc42-specific GEF and also known as p21-activated kinase-interacting exchange factor-αPIX, from the leading edge of the cell by disrupting the association between Pdlim5 and Arhgef6. Displacement of Arhgef6 suppresses Rac1 activity and the disappearance of Arp2/3 complex from the cell periphery, leading to defects in lamellipodia formation and inhibition of directional cell migration. We propose that Pdlim5 is the main signalling molecule that regulates cell migration in the context of augmented AMPK activity.

Results

Pdlim5 is phosphorylated at Ser177 by AMPK. Our group has worked on AMPK for many years. To estimate the AMPK activity level *in vivo*, we often monitor phospho-acetyl-CoA carboxylase (pACC), a well-known substrate of AMPK whose level generally reflects the AMPK activity[4]. When we treated C2C12 cells with AMPK activators such as 5-aminoimidazole-4-carboxyamide ribonucleoside (AICAR), A-769662 and 2-deoxy-D-glucose (2-DG), we serendipitously observed reproducible and specific induction of a protein with an apparent molecular mass of 64 kDa (p64) that cross-reacted with a commercially available antibody against pACC (Fig. 1a and Supplementary Fig. 1a,b, respectively). Three-step column chromatography followed by mass-spectrometric analysis revealed that p64 was likely to be Pdlim5 (ref. 19; Fig. 1b,c). To confirm this, we generated three polyclonal antibodies against mouse Pdlim5 (Supplementary Fig. 1c) and designed two different small interfering RNAs (siRNAs) against the *Pdlim5* messenger RNA (Supplementary Fig. 1d). When we treated C2C12 cells with siPdlim5, the p64 band disappeared (Fig. 1d). Therefore, we concluded that p64 is indeed Pdlim5. Furthermore, as the p64 band, probably representing a phosphorylated form of Pdlim5, was detected exclusively after AMPK activation, we speculated that Pdlim5 is a substrate of AMPK. Pdlim5, also known as Enigma homolog protein, is an α-actinin-binding protein that possesses a PDZ domain at its amino terminus and three LIM motifs at its carboxy terminus[19]. Pdlim5 anchors to the actin cytoskeleton via its PDZ domain and recruits LIM-associated proteins to actin filaments[20]. To narrow down the location of the phosphorylation site, we transfected wild-type (WT) Pdlim5 or deletion mutants (Supplementary Fig. 2a) into HEK293T cells, and then treated the transfectants with AICAR. A mutant truncated after N184 cross-reacted with the pACC antibody following AMPK activation (Supplementary Fig. 2b), whereas a mutant truncated after N160 did not, indicating that the phosphorylation site resides within the N-terminal segment of Pdlim5 between Ala161 and Asn184.

Next, we introduced Ser-to-Ala or Thr-to-Ala point mutations into this putative phosphorylation segment (Fig. 2a). Both the S175A and S177A mutants lost cross-reactivity with pACC antibody (Fig. 2a). Next, we performed *in vitro* phosphorylation assays on recombinant FLAG-tagged Pdlim5 (WT, S175A and S177A). The results revealed that incorporation of [γ-^{32}P]ATP into Pdlim5 was inhibited only in the S177A mutant, indicating that Ser177 is the unique phosphorylation site of Pdlim5 (Fig. 2b). We confirmed direct phosphorylation of Pdlim5 at Ser177 by AMPK by *in vitro* phosphorylation assay using recombinant glutathione *S*-transferase (GST)-fused Pdlim5 (WT or S177A) expressed in *Escherichia coli* (Supplementary Fig. 2c,d), and subsequently by using an antibody we generated (Supplementary Fig. 2e) against Ser177-phosphorylated Pdlim5 (Ab-pS177) (Fig. 2c). The amino-acid sequence surrounding Ser177 matches the consensus sequence for AMPK phosphorylation sites (Supplementary Fig. 2f) and also exhibits a high similarity with the phosphorylation site of ACC (Supplementary Fig. 2f). Furthermore, Ser177, but not Ser175, is highly conserved only in mammals (Supplementary Fig. 3). Next, we confirmed that endogenous Pdlim5 is phosphorylated at Ser177 on AMPK activation *in vivo* in vascular smooth muscle cells (vSMCs) (Fig. 2d and Supplementary Fig. 4). Finally, we investigated whether Pdlim5 is phosphorylated in response to an acute physical stimulus. Hypoxia (1% O_2 for 2 h) activated AMPK and induced Ser177-phosphorylation of Pdlim5 (Fig. 2e). Together, these data indicated that augmented AMPK activity induces Ser177 phosphorylation of Pdlim5 both *in vitro* and *in vivo*.

Ser177 phosphorylation of Pdlim5 inhibits cell migration. To accurately assess the functions of Ser177 phosphorylation of Pdlim5 by AMPK, it is essential to use a system that eliminates any effects associated with AMPK activation other than Ser177 phosphorylation. For this purpose, we established the knockdown-rescue (KDR) system in vSMCs by depleting endogenous Pdlim5 and simultaneously expressing siPDLIM-resistant enhanced green fluorescent protein (EGFP)-tagged Pdlim5 (Fig. 3a). For this purpose, we treated cells with siRNA oligonucleotides targeting the 3′-untranslated region mRNA of mouse Pdlim5 (siPdlim5-2) and infected them with adenovirus encoding EGFP-WT-, EGFP-S177A- or EGFP-S177D-Pdlim5, yielding cells we designated KDR/WT-, KDR/S177A- or KDR/

© 2015 Macmillan Publishers Limited. All rights reserved.

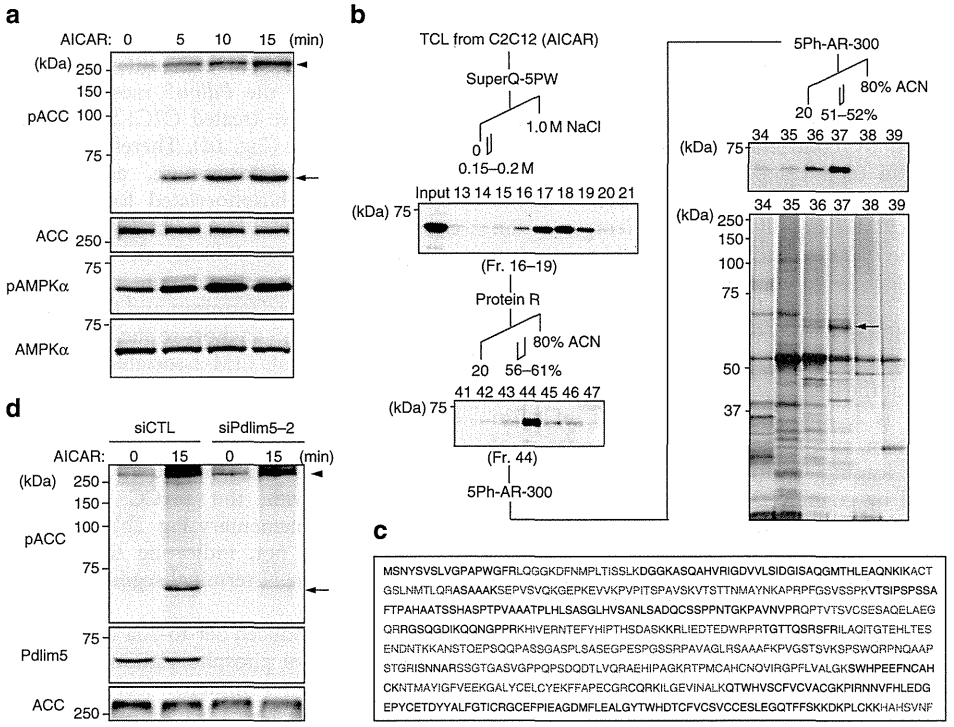

Figure 1 | Pdlim5 is a substrate of AMPK. (**a**) C2C12 cells were stimulated with AICAR (2 mM) 12 h after serum starvation. Total cell lysates (TCLs) were harvested 0, 5, 10 and 15 min after stimulation and subjected to immunoblotting with anti-pACC antibody. In addition to the predicted band for pACC (arrowhead), a cross-reacting band, p64 (arrow), was detected in a time-dependent manner after AICAR treatment. (**b**) A schematic representation of the purification and identification of p64. TCLs from C2C12 cells treated with AICAR were subjected to three-step column chromatography (superQ-5PW, protein R and 5Ph-AR-300). p64 was detected using the anti-pACC antibody in each step. Images were obtained by immunoblotting and silver staining. The identified band (arrow in silver-stained gel), fractionated by reverse-phase HPLC (5Ph-AR-300), was excised and analysed by mass spectrometry. (**c**) Amino acid sequence of Pdlim5. Sequence analysis by MALDI-Qq-TOF MS/MS revealed the target protein to be Pdlim5. Matching amino acids are shown in magenta letters. (**d**) C2C12 cells treated with siRNA (siCTL or siPdlim5-2) were stimulated with AICAR and TCLs were subjected to immunoblotting with pACC and Pdlim5 antibodies (Ab229-2). Arrowhead and arrow denote pACC and p64, respectively.

S177D-Pdlim5, respectively. This KDR system successfully replaced endogenous Pdlim5 with EGFP-Pdlim5 at physiological expression levels in vSMCs (Fig. 3a). Exogenously expressed EGFP-Pdlim5 co-localized with α-actinin and F-actin structures (Fig. 3b), a pattern similar to that of endogenous Pdlim5 (Supplementary Fig. 5), although EGFP-Pdlim5 appeared in the cytoplasm at much higher levels than the endogenous protein. Importantly, EGFP-WT-Pdlim5 was phosphorylated by AMPK in the same manner as endogenous Pdlim5, whereas EGFP-S177A-Pdlim5, an unphosphorylatable mutant, was not phosphorylated (Fig. 3c). EGFP-S177D-Pdlim5, a phosphomimetic mutant, was recognized by the Ab-pS177 antibody even in the absence of AICAR stimulation (Fig. 3c). This result indicates that phosphorylated WT-Pdlim5 and the S177D-Pdlim5 mutant are structurally similar. Thus, even in the absence of AMPK activators, exogenously expressed EGFP-S177D-Pdlim5 behaved similar to endogenous Pdlim5 phosphorylated by AMPK. It is particularly noteworthy that the KDR system can exclude any effects associated with AMPK activation other than Ser177 phosphorylation of Pdlim5.

AMPK activation inhibits cell migration; to investigate whether this effect is mediated by Pdlim5 phosphorylation at Ser177, we performed a scratch assay using the KDR/vSMC system in the absence of AMPK activators. KDR/S177D-Pdlim5 cells exhibited a marked delay in scratch closure relative to both KDR/WT- and KDR/S177A-Pdlim5 cells (Fig. 3d,e and Supplementary Movie 1). By tracking the movement of individual cells, we could calculate the path length (L) and displacement (D) of individual cells (Fig. 3f). KDR/S177D-Pdlim5 cells exhibited a lower migration speed (defined as L/total trajectory time) and less directionality (defined as D/L) than KDR/WT- and KDR/S177A-Pdlim5 cells (Fig. 3g,h). Next, we performed a scratch assay in the presence of AMPK activator (Supplementary Fig. 6). Compared with KDR/WT- and KDR/S177D-Pdlim5 cells, the degree of cell migratory inhibition was lower in KDR/S177A-Pdlim5 cells (Supplementary Fig. 6). Furthermore, we examined single-cell migration in the absence of AMPK activators. Consistent with the results of the scratch assay, KDR/S177D-Pdlim5 cells exhibited impaired cell migration (Supplementary Fig. 7a,b and Supplementary Movie 2).

Next, we examined the AMPK specificity of the phenotypes observed in KDR cells using AMPKα1$^{-/-}$α2$^{-/-}$ mouse embryonic fibroblasts (AMPKα-null MEFs). First, we confirmed that Pdlim5 phosphorylation by AMPK activators was completely blocked in AMPKα-null MEFs (Fig. 4a and Supplementary Fig. 8). Moreover, a scratch assay confirmed that AMPK activator-induced cell migratory inhibition was abolished in AMPKα-null MEFs (Fig. 4b–d and Supplementary Movie 3). For further confirmation, we constructed a Pdlim5 knockout vSMC (Pdlim5$^{-/-}$ vSMC) line by genome editing, using the CRISPR/Cas9 system (Supplementary Fig. 9), and established a knockout and rescue cell system by expressing EGFP-Pdlim5 (WT, S177A or S177D) at physiological level by adenovirus transduction of knockout cells (Supplementary Fig. 10a). When the knockout and rescue cells were subjected to a cell migration assay (Supplementary Fig. 10b–d), the results were consistent with

© 2015 Macmillan Publishers Limited. All rights reserved.

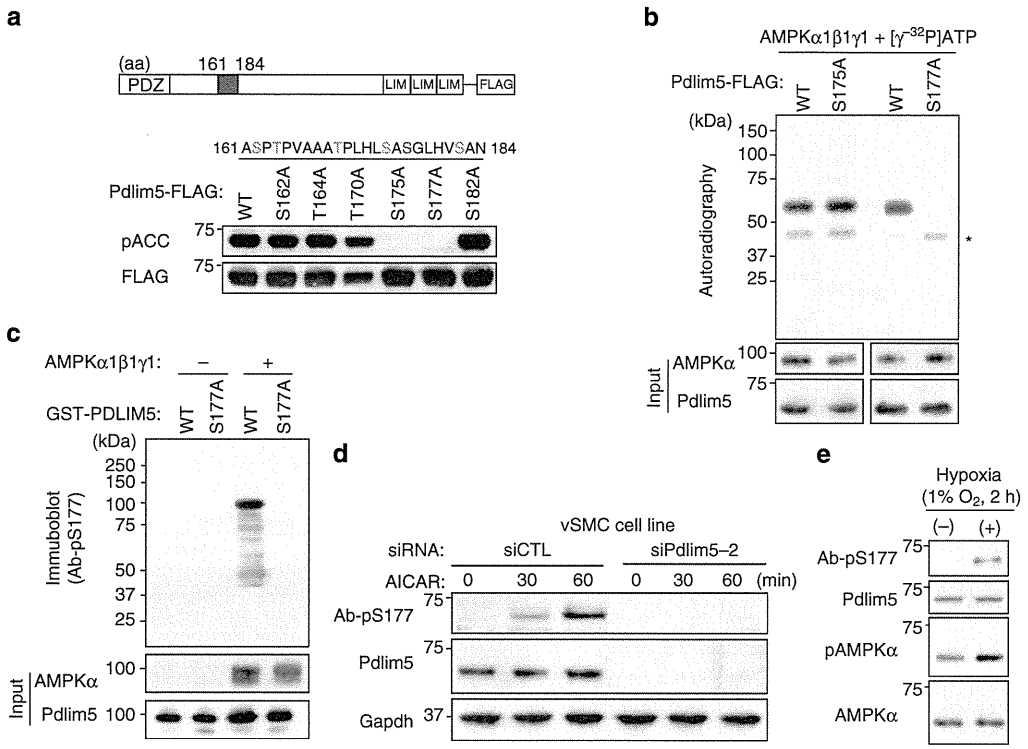

Figure 2 | Pdlim5 is directly phosphorylated at Ser177 by AMPK. (**a**) Diagrams of point-mutated Pdlim5. HEK293T cells were transiently expressed with each point-mutant of cFLAG-tagged Pdlim5 and treated with AICAR (2 mM) for 15 min. Proteins purified on anti-FLAG M2 agarose were subjected to immunoblotting with anti-pACC or anti-FLAG antibody. (**b**) *In vitro* assay for AMPK phosphorylation. Recombinant cFLAG-tagged Pdlim5 (WT, S175A or S177A) from HEK293T cells was incubated with baculovirus-expressed recombinant AMPK in the presence of [γ-^{32}P]ATP and then subjected to autoradiography. Asterisk denotes bands of α-subunit of recombinant AMPK. (**c**) *In vitro* phosphorylation assay by AMPK. Recombinant GST-tagged Pdlim5 proteins (WT and S177A) were incubated with or without recombinant AMPK and then subjected to immunoblotting with Ab-pS177. (**d**) vSMCs transfected either with siCTL or siPdlim5-2 were treated with AICAR (2 mM) for the indicated times, and TCLs were subjected to immunoblotting with Ab-pS177. (**e**) vSMCs were exposed to physiological hypoxia (1% O_2 for 2 h). TCLs were subjected to immunoblotting with the indicated antibodies.

those obtained with the KDR cells. Together, these results indicated that Ser177 phosphorylation of Pdlim5 by AMPK inhibits cell migration.

Ser177 phosphorylation altered actin architectures. To elucidate the mechanism by which Ser177 phosphorylation of Pdlim5 inhibits cell migration, we monitored morphological changes in KDR cells. In all three types of KDR cells, EGFP-Pdlim5 protein co-localized with F-actin at the cell periphery and on stress fibres (Fig. 5a), indicating that co-localization of Pdlim5 with actin was not influenced by the phosphorylation state of Ser177. However, KDR/WT- and KDR/S177A-Pdlim5 cells displayed smooth lamellipodia-like edges, whereas KDR/S177D-Pdlim5 cells exhibited attenuated lamellipodia formation and jagged edges with excessive filopodia-like protrusions and ventral stress fibres (Fig. 5a and Supplementary Fig. 11a). In addition, both KDR/WT- and KDR/S177A-Pdlim5 cells contained small and scattered spots of focal adhesions at the junction between the lamellipodia and lamella; by contrast, in KDR/S177D-Pdlim5 cells, focal adhesions were displaced to the edge of the cell and significantly enlarged in size (Fig. 5a and Supplementary Fig. 11b). To determine whether the morphological changes observed in KDR/S177D-Pdlim5 cells were related to Ser177 phosphorylation of Pdlim5, we performed time-lapse imaging before and after treatment with AMPK activator (Fig. 5b,c). In KDR/WT-Pdlim5 cells, but not in KDR/S177A-Pdlim5 cells, AMPK activation induced defective lamellipodia formation and promoted expansion of the EGFP signals from the side opposite the lamellae towards the cell centre (Fig. 5b,c and Supplementary Movie 4), a pattern resembling the growth of dorsal stress fibres. This morphological change was similar to that observed in KDR/S177D-Pdlim5 cells. Furthermore, AMPK activation induced defective lamellipodia and enhanced stress fibre formation in WT-MEFs, but not AMPKα-null MEFs (Fig. 4e). These findings suggested that Ser177 phosphorylation of Pdlim5 by augmented AMPK activity induced attenuation of lamellipodia and promoted formation of stress fibres from the cell periphery. Furthermore, these observations suggested that morphological changes of the actin architecture were initiated near the cell periphery.

Ser177 phosphorylation altered Arp2/3 complex localization. Accordingly, we focused on the Arp2/3 complex, because it is one of the major actin nucleators at the cell periphery and plays a key role in lamellipodia formation[10]. Expression levels of Arp2/3 complex were comparable among the various types of KDR cells (Supplementary Fig. 12a). However, the intracellular localization of Arp2/3 complex was markedly altered in both spreading and polarized cells (Fig. 6). In spreading cells, KDR/WT-Pdlim5 cells exhibited highly uniform lamellipodia throughout the cell edge, where Arp3 predominantly localized (Fig. 6a). By contrast, KDR/S177D-Pdlim5 cells exhibited filopodia-like protrusions instead of lamellipodia, and localization of Arp3 shifted from the cell edge to a cytoplasmic distribution (Fig. 6a). A similar pattern was observed in polarized cell: Arp3 localized in actin-rich

© 2015 Macmillan Publishers Limited. All rights reserved.

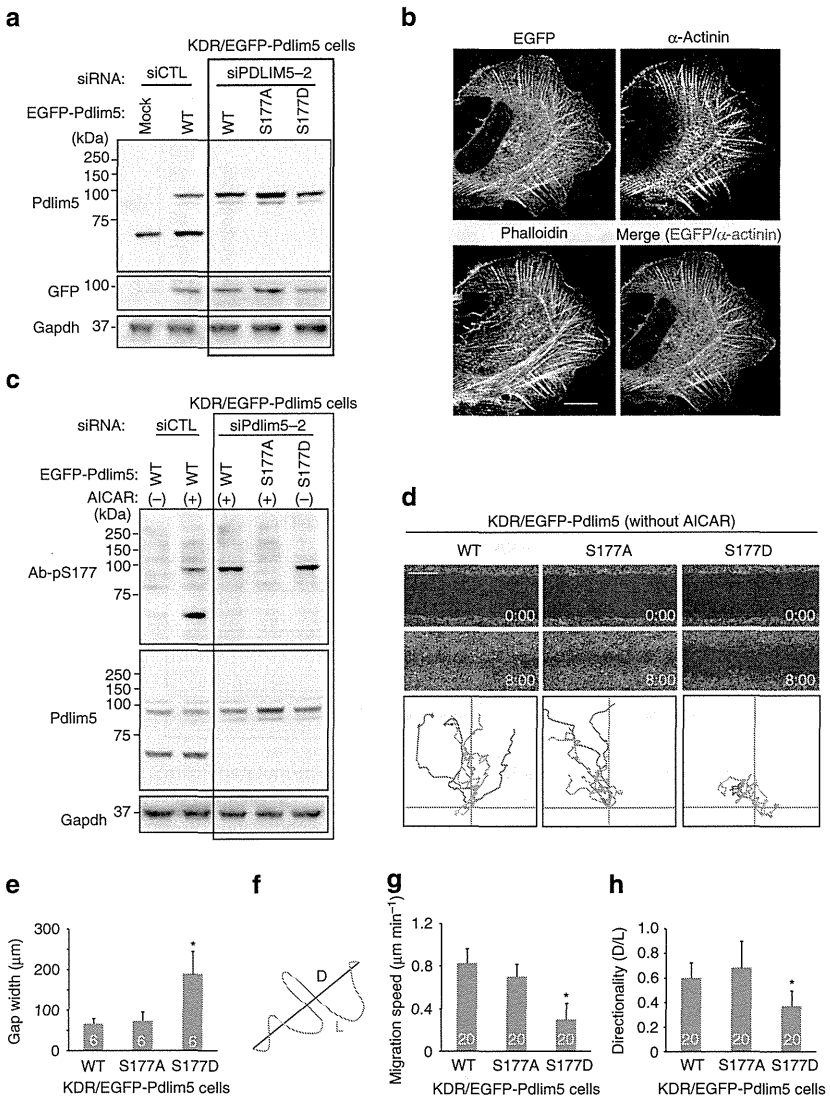

Figure 3 | Ser177 phosphorylation of Pdlim5 by AMPK inhibited directional migration of vSMCs. (**a**) Establishment of the KDR system for Pdlim5 in vSMCs. vSMCs were transfected with either siCTL or siPdlim5-2. siPdlim5-2-resistant EGFP-Pdlim5 (WT, S177A or S177D) was added back by adenoviral-mediated gene delivery. TCLs were subjected to immunoblotting. (**b**) GFP and immunostained images of KDR/EGFP-WT-Pdlim5 cells stained with a α-actinin antibody and phalloidin. Scale bar, 10 μm. (**c**) KDR/EGFP-Pdlim5 (WT and S177A) cells were treated with AICAR for 60 min, whereas KDR/EGFP-S177D-Pdlim5 cells were not treated with AICAR. TCLs from each cell were subjected to immunoblotting. (**d**) Scratch assay of KDR/EGFP-Pdlim5 cells. Phase-contrast microscopy images of KDR/Pdlim5 cells (WT, S177A and S177D) before and 8 h after scratching in the absence of AICAR. The bottom row of each panel shows analysis of migration paths over 8 h. The origins of migration of each cell were superimposed at [0, 0]. Scale bar, 0.5 mm. (**e**) Bar graph showing the gap width 8 h after scratching (from **d**). (**f**) Demonstration of path length (L) and displacement (D) for calculation of migration velocity and directionality. (**g**) Bar graph showing migration speed of each cell (from **d**). (**h**) Bar graph showing migration directionality of each cell (from **d**). Numbers in the bars indicate *n*. Data are representative of means ± s.e.m. from three independent experiments. Significance of differences between series of results was assessed using one-way analysis of variance, followed by a *post-hoc* comparison with Dunnett's method for multiple comparisons. $^{*}P<0.01$ compared with WT.

lamellipodia in KDR/WT-Pdlim5 cells, but was distributed diffusely throughout the cytoplasm in KDR/S177D-Pdlim5 cells (Fig. 6b). These findings indicated that Ser177 phosphorylation of Pdlim5 impairs the function of the Arp2/3 complex by altering the localization of the complex from the cell edge to the cytoplasm. Consistent with this, vSMCs defective for Arp2/3 complex due to knockdown of the Arpc2 subunit exhibited a phenotype very similar to that of DR/S177D-Pdlim5 cells (Supplementary Fig. 12b,c). On the other hand, mammalian diaphanous (mDia), another actin nucleator, persisted at the leading edge of the cells (Supplementary Fig. 13).

Ser177 phosphorylation of Pdlim5 decreased Rac1 activity. Next, we measured the activities of Rac1, an upstream regulator of the Arp2/3 complex that is required for lamellipodia formation[8,9]. GTP-bound active Rac1 was significantly reduced in KDR/S177D-Pdlim5 cells relative to KDR/WT- and KDR/S177A-Pdlim5 cells (Fig. 7a). Furthermore, we carried out imaging of Rac1 activity in living cells, using vSMCs stably expressing the Raichu-Rac1 probe (vSMC-R_{Rac1} cells), which is based on the principle of fluorescence resonance energy transfer (FRET) biosensors[21]. We established the KDR system in vSMC-R_{Rac1} cells, as described above, except that siPDLIM-resistant Pdlim5

© 2015 Macmillan Publishers Limited. All rights reserved.

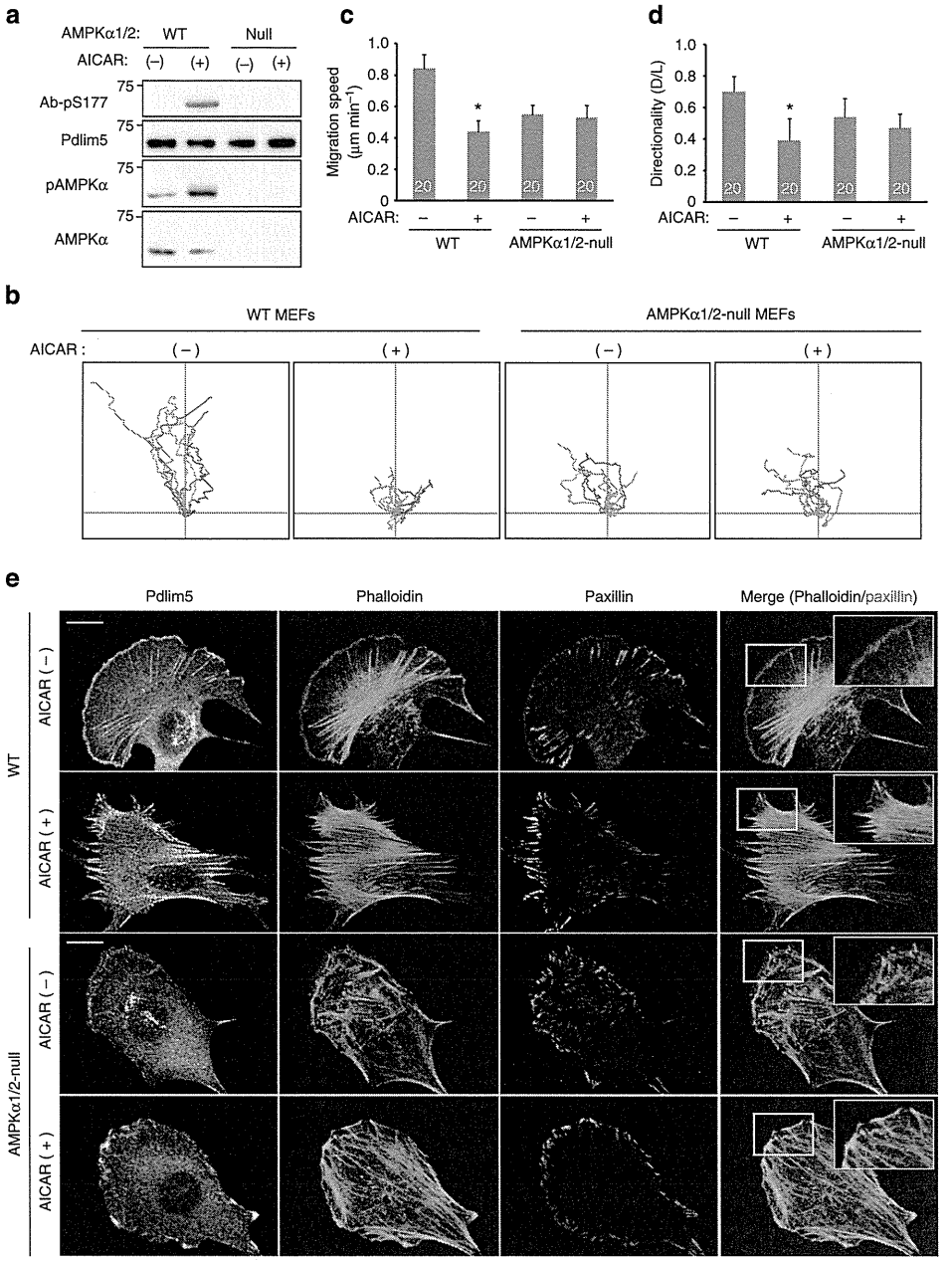

Figure 4 | Pdlim5 phosphorylation was blocked in AMPKα1/2-null MEFs. (**a**) WT or AMPKα1/2-null MEFs were stimulated with AICAR (1 mM) for 15 min. TCLs were subjected to immunoblotting with indicated antibodies. (**b**) Phase-contrast images of WT-MEFs and AMPKα1/2-null MEFs were collected during the scratch assay in the presence or absence of AICAR (1 mM). Each panel shows analysis of migration paths over 8 h. The origins of migration of each cell were superimposed at [0, 0]. (**c**) Bar graph showing the migrating speed of each cell (from **b**). (**d**) Bar graph showing migration directionality of each cell (from **b**). Numbers in the bars indicate *n*. Data are representative of means ± s.e.m. from three independent experiments. Significance of differences between series of results was assessed using one-way analysis of variance, followed by a *post-hoc* comparison with Dunnett's method for multiple comparisons. *$P<0.01$ compared with WT without AICAR treatment. (**e**) Immunostained images of WT-MEFs and AMPKα1/2-null MEFs in the presence or absence of AICAR (1 mM). These cells were stained with a Pdlim5 antibody, phalloidin and anti-paxillin antibody. Magnified images outlined by yellow squares show the areas outlined by white squares. Scale bar, 10 μm.

was co-expressed with mCherry instead of being tagged with EGFP (Raichu-Rac1/KDR/Pdlim5-T2A-mCherry) (Fig. 7d). Rac1 activity was lower in cells expressing S177D-Pdlim5 than in those expressing WT-Pdlim5 or S177A-Pdlim5, especially in the cell periphery (Fig. 7e and Supplementary Fig. 14). Thus, these findings indicated that Rac1 activity was suppressed in cells expressing S177D-Pdlim5, especially in the cell periphery, resulting in dislocation of the Arp2/3 complex. On the other hand, we observed no changes in RhoA or Cdc42 activity (Fig. 7b,c and Supplementary Fig. 15).

Pdlim5 phosphorylation altered the interaction with Arhgef6. To investigate the molecular mechanism by which S177D-Pdlim5 suppresses Rac1 activity, we performed GST pull-down assays followed by high-sensitivity shotgun liquid chromatography–mass

© 2015 Macmillan Publishers Limited. All rights reserved.

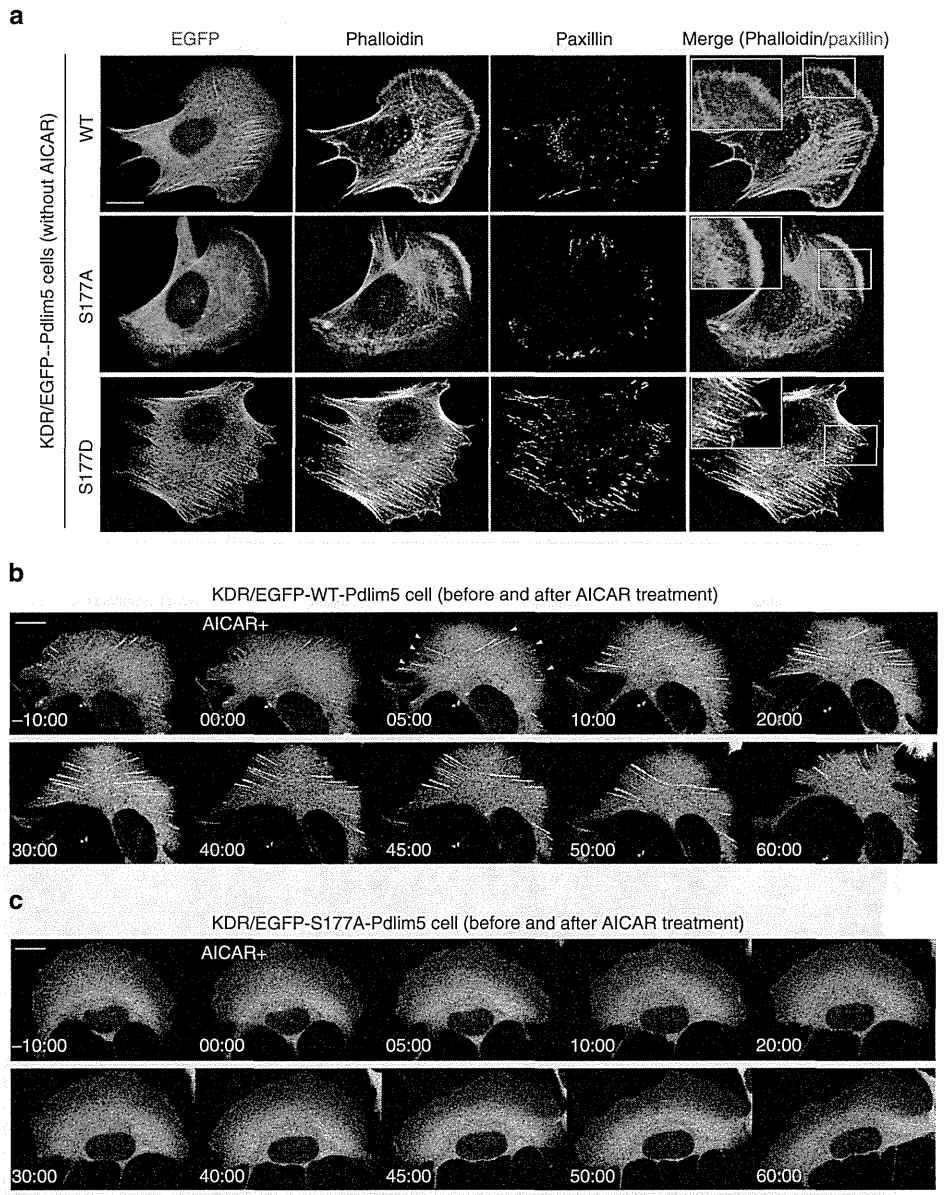

Figure 5 | Ser177 phosphorylation of Pdlim5 causes reorganization of lamellipodia, stress fibres and focal adhesions. (**a**) GFP images (left) and immunostained images of KDR/EGFP-Pdlim5 cells (WT, S177A and S177D). Cells were stained with phalloidin and anti-paxillin antibody, to visualize actin microfilaments and focal adhesions, respectively. Magnified images outlined by yellow squares show the area outlined by the white squares. Scale bar, 10 μm. (**b**,**c**) Sequential GFP images of KDR/EGFP-WT-Pdlim5 (**b**) or KDR/EGFP-S177A-Pdlim5 (**c**) cells before and after AICAR stimulation (2 mM). Yellow arrowheads represent dorsal stress fibres growing from the opposite side after AICAR treatment of KDR/EGFP-WT-Pdlim5 cells. Scale bar, 10 μm.

spectrometry, using total cell lysates from U937 cells. Among a total of 1,225 proteins detected, several RhoGEFs were more prominently associated with GST-WT-Pdlim5 than with GST-S177D-Pdlim5 (Supplementary Table 1). Among them, we focused on Arhgef6, because it exclusively associated with WT-Pdlim5 (Fig. 8a) and can activate Rac1 at the leading edge of migrating cells[22,23]. Both the biochemical dissociation of Arhgef6 and S177D-Pdlim5, and the intracellular co-localization of Arhgef6 with Pdlim5 at the cell periphery were disrupted in KDR/S177D-Pdlim5 cells (Fig. 8b). These findings suggested that Ser177 phosphorylation of Pdlim5 disrupted the recruitment of Arhgef6 at the cell's leading edge, potentially suppressing Rac1 activity. Next, we compared the effect of Arhgef6 knockdown on cell migration and morphology with that of Ser177 phosphorylation of Pdlim5 (Fig. 8c and Supplementary Fig. 16). The similarity was only partial: Arhgef6-knockdown vSMCs exhibited a disturbed migration relative to control vSMCs (Supplementary Fig. 16b–d) and defective lamellipodia (Fig. 8c), but not elevated formation of stress fibres (Fig. 8c).

Pdlim5 recruits AMPK onto actin filaments. To investigate how AMPK signalling is transmitted to peripheral actin filaments, we examined the physical link between actin filaments, Pdlim5 and AMPK. Immunoprecipitation/immunoblotting of HEK293T cells co-transfected with V5-tagged AMPKα and FLAG-tagged Pdlim5 (WT, ΔPDZ or ΔLIM) demonstrated that AMPK bound to Pdlim5 through the LIM domain (Fig. 9a). Next, we performed an F-actin-binding assay, in which F-actin and its binding proteins are found in the pellet fraction, to determine whether Pdlim5

© 2015 Macmillan Publishers Limited. All rights reserved.

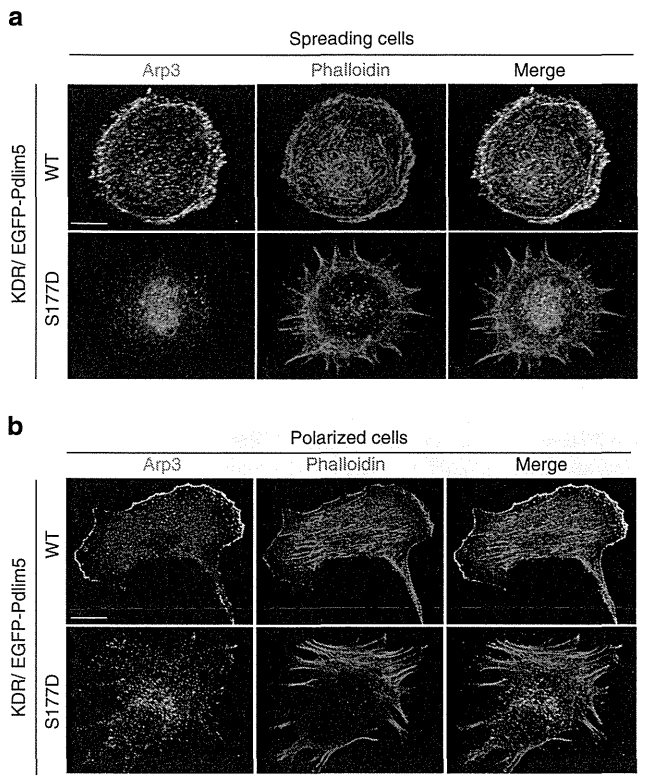

Figure 6 | Ser177 phosphorylation of Pdlim5 leads to altered Arp2/3 complex localization. (**a**,**b**) Immunostaining of spreading (**a**) or polarized (**b**) KDR/EGFP-Pdlim5 cells. Cells were fixed and stained with an Arp3 antibody and phalloidin. Scale bars, 10 μm.

promotes the recruitment of AMPK onto actin filaments. In the absence of Pdlim5, AMPK was found exclusively in the supernatant (Fig. 9b). However, in the presence of Pdlim5, AMPK shifted from the supernatant to the pellets and this shift was greatly stimulated by the presence of α-actinin (Fig. 9b). These findings indicate that Pdlim5 binds AMPK directly and promotes the recruitment of AMPK onto F-actin, a process mediated by α-actinin.

Discussion

The results described here reveal the mechanism by which augmented AMPK activity inhibits cell migration. In this study, we serendipitously identified Pdlim5 as a novel substrate of AMPK. On augmentation of AMPK activity, Pdlim5 was phosphorylated at Ser177, disrupting its association with Arhgef6 at the cell periphery and suppressing Rac1 activity at the leading edge of cell. Suppression of Rac1 activity dislocated the Arp2/3 complex from the leading edge, resulting in attenuation of lamellipodia formation and inhibition of cell migration.

We previously established a unique screening method using two-step column chromatography combined with an *in vitro* kinase reaction. Using this method, we identified CLIP-170 as a novel AMPK substrate[4]. In this study, we identified Pdlim5 as another substrate of AMPK by probing cells with a pACC antibody after AMPK activation. The amino-acid sequence surrounding Ser177 of Pdlim5 is very similar to a sequence in ACC, which may explain why we were able to discover this new AMPK substrate using a pACC antibody. Importantly, Pdlim5 is not phosphorylated at all before stimulation with AMPK activators, whereas other AMPK substrates such as ACC and CLIP-170 (ref. 4) are already phosphorylated to some extent even before stimulation. These findings suggest that Pdlim5 is phosphorylated only under stressed conditions in which AMPK activity is augmented. Accordingly, we conclude that the functional impact of Pdlim5 phosphorylation by AMPK is exerted only under cellular conditions associated with augmented AMPK activity. Thus, Pdlim5 phosphorylation might cause different biological effects than phosphorylation of other AMPK substrates.

In mouse, the double knockout of AMPKα1α2 (AMPKα1$^{-/-}$α2$^{-/-}$) is early embryonic lethal[24], but AMPKα-null MEFs are viable[25]. AMPK-null cells exhibit a metabolic shift towards aerobic glycolysis[26], as well as abnormalities in cell polarity and cellular structures[2]. Pharmacological inhibition of AMPK also perturbs cell polarity and migration[4]. Thus, it is reasonable to conclude that AMPK activity affects directional cell migration by regulating cell polarity. However, as AMPK has many substrates other than Pdlim5, it is still difficult to infer the role of Pdlim5 phosphorylation from the lethal phenotype of the AMPKα1$^{-/-}$α2$^{-/-}$ mouse. On the other hand, two studies have reported different phenotypes of Pdlim5 homozygous knockout mice: dilated cardiomyopathy[27] and embryonic lethality probably due to embryonic heart/circulation failure[28]. Pdlim5 associates with the actin cytoskeleton and promotes the assembly of protein complexes by acting as a scaffold protein, and thus recruit proteins that modulate cell architecture, actin dynamics and signal transduction[19] to the actin filaments. Therefore, both phenotypes of Pdlim5 homozygous knockout mice may be attributed to the loss of organized cytoskeletal structures due to progressive loss of protein complex components. Similarly, we postulate that Pdlim5 and its phosphorylation play an important role in regulation of cell morphology and migration, although no previous reports have described the cell migratory behaviour of Pdlim5-knockout cells.

In this study, we focused on determining how AMPK-induced Ser177 phosphorylation of Pdlim5 inhibits cell migration. We found that Pdlim5 localized on actin-filament structures such as stress fibres and focal adhesions, as well as at the cell cortex (including lamellipodia), and that Ser177 phosphorylation itself did not influence Pdlim5 localization. However, the phosphomimetic mutant S177D-Pdlim5 caused characteristic morphological changes such as defective lamellipodia, enhanced ventral stress fibres and displacement of focal adhesions to the cell edge. These specific morphological changes at the cell edge were also observed on pharmacological activation of endogenous AMPK. Thus, the major initial morphological changes resulting from Ser177 phosphorylation of Pdlim5 seemed to arise from the cell cortex. Arhgef6 belongs to the Dbl family of GEFs, defined by the presence of tandem Dbl homology and Pleckstrin homology domains, and functions as a Rac-specific GEF at the cell periphery[22,23,29]. Arhgef6 is recruited to a signalling complex consisting of integrin-linked kinase, particularly interesting cysteine–histidine-rich protein and parvin (IPP complex) by binding to parvin[30,31] (Fig. 10), which plays an important role in cell spreading and motility[32], and may be involved in the Pdlim5 phosphorylation signal mediated by Arhgef6. The IPP complex assembles at small focal complexes at the tips of lamellipodia of migrating cells and then interacts with the cytoplasmic tails of β-integrin molecules to connect them to the actin cytoskeleton[32]. Thus, Arhgef6 activates Rac1 and reorganizes the actin cytoskeleton around the focal complex of lamellipodia, which is necessary for cell spreading and migration[29]. Moreover, α-actinin also binds to parvin directly[33] and is involved in the IPP complex[31]. As Pdlim5 binds to α-actinin directly[34], it is likely to be that Pdlim5 is recruited to the IPP complex in close proximity to Arhgef6 via binding to α-actinin. It is particularly noteworthy

© 2015 Macmillan Publishers Limited. All rights reserved.

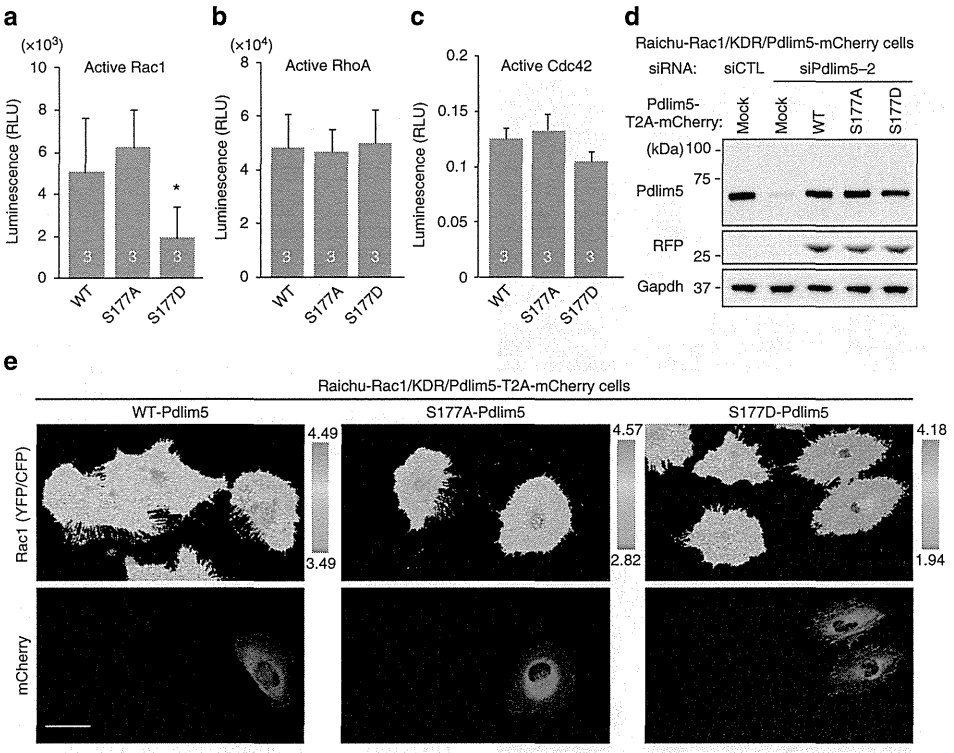

Figure 7 | Ser177 phosphorylation of Pdlim5 suppressed Rac1 activity. (**a–c**) Activities of Rac1 (**a**), RhoA (**b**) and Cdc42 (**c**) in KDR cells were quantitated using G-LISA specific for Rac1, RhoA and Cdc42, respectively. Numbers in the bars indicate *n*. Data are representative of means ± s.e.m. from three independent experiments. Significance of differences between series of results was assessed using one-way analysis of variance, followed by a *post-hoc* comparison with Dunnett's method for multiple comparisons. $*P<0.01$ compared with KDR/EGFP-WT-Pdlim5. (**d**) The KDR system was established in vSMCs stably expressing FRET probes specific for Rac1 (Raichu-Rac1/vSMCs). Raichu-Rac1/vSMCs were transfected with either siCTL or siPdlim5-2. siPdlim5-2-resistant Pdlim5-T2A-mCherry (WT, S177A and S177D) was introduced via adenoviral-mediated gene delivery (Raichu-Rac1/KDR-Pdlim5-T2A-mCherry cells). TCLs were subjected to immunoblotting. (**e**) Imaging of Rac1 activity. Each type of Raichu-Rac1/KDR-Pdlim5-T2A-mCherry cell (WT, S177A and S177D) was imaged for YFP and CFP. FRET efficiencies are shown as YFP/CFP ratio images. Scale bars, 20 μm.

that S177D-Pdlim5 disrupted the physical association between Pdlim5 and displaced Arhgef6 from the cell periphery (Fig. 8). These findings led us to speculate that Arhgef6 is displaced from the IPP complex on Ser177 phosphorylation of Pdlim5 by AMPK, resulting in the suppression of Rac1 activity at the cell's leading edge. Rac1 is predominantly localized at the plasma membrane[35] and GTP-bound active Rac1 at the cell periphery can activate Arp2/3 complex through recruitment of the Wiskott–Aldrich Syndrome protein family verprolin homologous complex[10,11]. Therefore, we expected that the function of Arp2/3 complex would also be suppressed in KDR/S177D-Pdlim5 cells. In fact, the Arp2/3 complex was displaced from the cell periphery and distributed throughout the cytoplasm in KDR/S177D-Pdlim5 cells, consistent with a previous study demonstrating that inhibition of Rac1 activity interferes with intracellular localization of the Arp2/3 complex[36]. Furthermore, the morphological characteristics observed in KDR/S177D-Pdlim5 cells were quite similar to those in cells with a functional defect in the Arp2/3 complex[37–39]. As Arp2/3 complexes play a pivotal role in organizing branched actin filament networks to form lamellipodia[10,11], the attenuation of lamellipodia formation and inhibition of cell migration observed in KDR/S177D-Pdlim5 cells was plausible. Thus, our findings strongly suggest that Ser177 phosphorylation of Pdlim5 by AMPK suppresses Rac1 activity by displacing Afhgef6 from the cell periphery, leading to functional suppression of the Arp2/3 complex. However, as the morphological phenotype of Arhgef6-knockdown cells was not entirely consistent with that of KDR/S177D-Pdlim5 cells, we must consider the idea that mechanisms other than the Arhgef6–Rac1–Arp2/3 complex pathway contribute to the phenotypes resulting from Ser177 phosphorylation of Pdlim5. One possible mechanism involves a relative increase in RhoA activity over Rac1 due to a reduction in Rac1 activity, which may contribute to the phenotype even in the absence of elevated RhoA activity. Consistent with this idea, the relative balance between Rac1 and RhoA activities regulates cell morphology and migratory behaviour[40,41]. Another possibility is that other GEFs or GTPase-activating proteins contribute to the phenotype of KDR/S177D-Pdlim5 cells. Indeed, dedicator of cytokinesis 2 is also a Rac-specific GEF and interacted with WT-Pdlim5 more strongly than with S177D-Pdlim5 (Supplementary Table 1).

Another important question relates to the mechanism underlying excessive formation of stress fibres, observed in both vSMCs treated with AMPK activator and KDR/S177D-Pdlim5 cells. In particular, cells stimulated with AMPK activators exhibited striking elongation of dorsal stress fibres from the cell periphery. This finding was in excellent agreement with a previous report demonstrating that Arp2/3-defective cells exhibited a higher growth rate of dorsal stress fibres[39]. The authors of that report proposed that the elevated growth of dorsal stress fibres may result from the increased concentration of cytoplasmic G-actin caused by the absence of Arp2/3-nucleated barbed ends[10]. In addition, mDia remained localized at the cell periphery in KDR/S177D-Pdlim5 cells, whereas Arp2/3 complex moved from the periphery to the cytosol. mDia is another major actin filament nucleator that nucleates linear actin filament at the cell periphery

© 2015 Macmillan Publishers Limited. All rights reserved.